CHAOS
Theory and Applications
in Applied Sciences and Engineering

e-ISSN: 2687-4539
RESEARCH ARTICLE
Vol.4 / No.4 / 2022 / pp.246-266
Special Issue (EDIESCA 2022)
https://doi.org/10.51537/chaos.1187427

Occurrence of Complex Behaviors in the Uncontrolled Passive Compass Biped Model

Essia Added [a,1], **Hassène Gritli** [a,b,2] **and Safya Belghith** [a,3]

[a]Laboratory of Robotics, Informatics and Complex Systems (RISC Lab, LR16ES07), National Engineering School of Tunis, University of Tunis El Manar, BP. 37, Le Belvédère, 1002 Tunis, Tunisia, [b]Higher Institute of Information and Communication Technologies, University of Carthage, 1164 Borj Cedria, Tunis, Tunisia.

ABSTRACT It is widely known that an appropriately built unpowered bipedal robot can walk down an inclined surface with a passive steady gait. The features of such gait are determined by the robot's geometry and inertial properties, as well as the slope angle. The energy needed to keep the biped moving steadily comes from the gravitational potential energy as it descends the inclined surface. The study of such passive natural motions could lead to ideas for managing active walking devices and a better understanding of the human locomotion. The major goal of this study is to further investigate order, chaos and bifurcations and then to demonstrate the complexity of the passive bipedal walk of the compass-gait biped robot by examining different bifurcation diagrams and also by studying the variation of the eigenvalues of the Poincaré map's Jacobian matrix and the variation of the Lyapunov exponents. We reveal also the exhibition of some additional results by changing the inertial and geometrical parameters of the bipedal robot model.

KEYWORDS
Compass biped robot
Passive dynamic walking
Poincaré map
Characteristic multipliers
Complexity
Chaos
Bifurcations
Bubbles
Lyapunov exponents

INTRODUCTION

The history of chaos theory began more than a century ago, in 1900, when mathematicians like Henri Poincaré studied the intricate motions of moving bodies (Walter 2014). Edward Lorenz finds the first chaotic weather system, sometimes known as an odd attractor, at the start of the 1960s. The paper "*Period three indicates chaos*" was an article written by Tien-Yien Li and James A. Yorke in 1975 that first used the word chaos (Li and Yorke 2004). And in 1990, James A. Yorke, Edward Ott, and Celso Grebogi introduced the idea of controlling chaos (Grebogi *et al.* 1997; Ott *et al.* 1990). The first application of chaos is the management of erratic behavior in systems and circuits (Andrievskii and Fradkov 2003, 2004). More applications and methods for analyzing and controlling chaos in engineering systems can be found for example in (Andrievskii and Fradkov 2003, 2004; Boccaletti *et al.* 2000; Fradkov and Evans 2005; Fradkov *et al.* 2006; Guanrong 2021; Harrison *et al.* 2022; Sprott 2020; Xiaoting *et al.* 2022; Yang and Zhou 2014).

Manuscript received: 16 October 2022,
Revised: 14 December 2022,
Accepted: 23 December 2022.

[1]addedessia@gmail.com
[2]grhass@yahoo.fr (**Corresponding author**)
[3]safya.belghith@enit.utm.tn

There are many applications for chaos (Andrievskii and Fradkov 2004; Boubaker and Jafari 2019; Grassi 2021; Jun 2022), but a few come to mind, such as in the engineering (Vibration control and circuit stabilization) (Akgul *et al.* 2016; Azar *et al.* 2017; Jimenez *et al.* 2009; Volos *et al.* 2017; Yang and Zhou 2014), in the computers (Encryption and packet switching in computer networks) (Beritelli *et al.* 2000). Additionally, in the world of medicine, there are techniques for analyzing heart rhythms (Ferreira *et al.* 2011), environment study (Aricioğlu and Berk 2022), enzyme-substrate reactions in a brain waves model via a biological snap oscillator (Vaidyanathan *et al.* 2018), predicting irregular heartbeats (Firth 1991), observation of performance of asynchronous machine (Öztürk 2020), stepper motor (Miladi *et al.* 2021), and controlling them. Moreover, in the field of mechanics and robotics, there are some applications of chaos in complex systems like the mechanical oscillators (Buscarino *et al.* 2016; Gritli and Belghith 2018a; Khraief Haddad *et al.* 2017), the mobile robots (Sambas *et al.* 2016; Vaidyanathan *et al.* 2017; Volos *et al.* 2012, 2013), and also the bipedal walking robots (Gritli and Belghith 2017a, 2018b; Iqbal *et al.* 2014; Montazeri Moghadam *et al.* 2018). The chaotic systems have been considered as important and attractive areas of research that have constantly evolved over the years which have an unpredictable behavior while changing the some parameters.

For a few years, the scientific community's and manufacturers' interest in mobile robotics has not waned. This sort of robot has a wide range of uses. There are primarily service robotics jobs (manoeuvrings, package distribution, and so on), as well as monitoring or obtaining information on the task environment of manufacturing carried out in a hostile or dangerous setting for humans (Bekey and Goldberg 2012).

In light of this, legged mobile robots have a lot of promise. The fundamental reason is that the employment of paws increases a mobile robot's overall mobility (Chevallereau *et al.* 2009; Goswami and Vadakkepat 2019; Meng and Song 2022). Indeed, only specifically equipped sites (roads, corridors, platforms) or areas with low inclination are accessible to a wheeled or tracked robot (fields, orchards). In steep situations, locations packed with obstructions on the ground, or urban spaces meant for people (issues with stairs, doorsteps, and side-walk), the legs are the optimum mode of locomotion. On rough floors, using the legs provides for a smoother movement and better performance than using the wheels (Meng and Song 2022).

Walking is a mode of locomotion for the lower limbs (the legs) of the body during which the subject always has at least one foot on the ground. This locomotion type gives birth to an alternation between the phase of simple support (one foot on the ground) and the phase of double support (two feet on the ground). Among biped walking mammals, human is the only one to adopt the erect attitude as its natural position that we want to imitate. Walking robots come in a variety of shapes and sizes: bipeds (Chevallereau *et al.* 2009; Reher and Ames 2021; Westervelt *et al.* 2007) and humanoids (Goswami and Vadakkepat 2019), etc.

McGeer developed a type of walking robots called passive dynamic walkers in the 1990s that can walk steadily down a slope without the aid of any actuators (McGeer 1990). In a lot of cases, impulsive hybrid nonlinear dynamics are used to describe bipedal walking robots (Chevallereau *et al.* 2009; Grizzle *et al.* 2001; Westervelt *et al.* 2007). Here, we are referring to impulsive mechanical systems that make stiff or even jarring interactions with particular surfaces. Using a biped robot that resembles a human is important to accurately examine the walking phenomenon. Particularly, articulated mechanical systems that experience collisions with the walking surface are designated as bipedal robots (Chevallereau *et al.* 2009; Westervelt *et al.* 2007).

In the present research work, we are interested in passive biped robots, and specially the compass-type bipedal robot, which is the simplest device that can more faithfully replicate human walking (Collins *et al.* 2005; Deng *et al.* 2017; Garcia *et al.* 2000, 1998; Kuo 2007; Miladi *et al.* 16-19 March 2015). It consists of two rigid legs with no knees and ankles, and it produces punctual contacts with the ground while walking.

The walk of a bipedal robot is modeled by a hybrid impulsive nonlinear dynamics (Fathizadeh *et al.* 2019; Goswami *et al.* 1998; Iqbal *et al.* 2014), which is considered complex and which can generate periodic cycles, quasi-periodic behaviors, chaotic motions and several types of bifurcation, including the period-doubling bifurcation, the cyclic-fold bifurcation, and the Neimark-Sacker bifurcation (called also the torus bifurcation), as for example in (Added and Gritli 2022, 2023; Added *et al.* 2021a,c; Fathizadeh *et al.* 2018; Goswami *et al.* 1998; Gritli and Belghith 2016a,b, 2017a,b, 2018b; Gritli *et al.* 2012, 2011, 2018; Jun 2022; Makarenkov 2020; Montazeri Moghadam *et al.* 2018; Nourian Zavareh *et al.* 2018). The existence and study of the period-doubling bifurcations exhibited in the biped robots' walking has been widely realized in the literature using the principle of Poincaré maps and also by determining its analytical expression like in (Znegui *et al.* 2020a, 2021) and also by using it in the chaos control (Znegui *et al.* 2020b). In (Added and Gritli 2022, 2023; Added *et al.* 2021b), a further study of the period-doubling bifurcations and their route to chaos has been realized. Moreover, in (Added and Gritli 2022), the numerical proof of the existence of the Neimark-Sacker bifurcation in the passive compass-gait bipedal robot has been achieved. The existence of such bifurcation has been demonstrated via only one set of parameters of the compass robot. In (Added *et al.* 2021a), an additional study of the complex motions of the passive bipedal gait of the compass walker has been realized using mainly bifurcation diagrams. Some unforeseen behaviors like the bubbles have been developed. A study of these behaviors and other motions including chaos, bifurcations and chaos in bubbles, has been also presented in (Added *et al.* 2021c).

The objective of this work is to further investigate the passive dynamic walking of the compass-type bipedal robot by mathematically modeling this dynamics for both phases: the swinging phase and the simple support phase, and simulating it numerically in order to observe the different complex behaviors. However, faced to the complexity of this task by observing chaos and bifurcations that appear for certain modification of the biped robot's parameters that has been recently started in (Added and Gritli 2022, 2023; Added *et al.* 2021a,b,c), then a thorough analysis of gait stability of the biped robot is necessary to proceed with and hence develop the analysis of this type of legged walking bipedal robots. We are then going to highlight the diversity of the complex behaviors covered by the fact of walking passively down sloped surfaces.

In previous articles, we have presented a variety of control methods based on tracking the passive dynamic walking and tracking a certain created trajectory with spline or Bezier functions (Added and Gritli 2020a,b; Added *et al.* 2021b, 2022a,b) to control the chaotic behavior in the bipedal walking of the compass-gait walker. Some other techniques like the OGY control and the delayed-feedback control methods have been widely employed for the suppression of chaos (Gritli *et al.* 2015, 2013; Iqbal *et al.* 2014; Znegui *et al.* 2020b).

Additionally, in order to analyze the walking behavior of the biped robot, it is crucial to apply the Poincaré map approach to determine therefore the fixed point for each walking gait due to the complexity of the impulsive hybrid nonlinear dynamics. By simulating this complex dynamics, an analysis of the behavior of the bipedal walking of the compass robot will be achieved by modifying its inertial and geometrical parameters and also the slope angle of the walking surface. Such analysis will be realized by means of the bifurcation diagrams that will reveal the presence of the period-doubling bifurcation, the Neimark-Sacker bifurcation, the cyclic-fold bifurcation and chaos. In addition, our analysis of the passive bipedal walking will be carried out by drawing the attractors in the phase planes and via the Poincaré section, and also by drawing the tendency of the eigenvalues of the Jacobian matrix of the Poincaré map. Some novel complex behaviors will be revealed in the bifurcation diagrams.

Our main contributions in this paper are summarized as follows:

- Analysis of chaos and bifurcations in the impulsive hybrid nonlinear dynamics of the passive dynamic walking of the compass bipedal robot under variation of two (bifurcation) parameters, namely the slope angle of the inclined walking surface and the length of the lower-half segment.
- Analysis and demonstration, via bifurcation diagrams, of existence of some period-doubling routes to chaos, period-

remerging scenario and bifurcation of bubbles (period bubbling).
- Investigation of the different motions by plotting and studying the resulting attractors in the phase planes and the Poincaré sections.
- Study of the stability of the period-1 walking gaits of the compass bipedal robot via the eigenvalues of the Jacobian matrix of the Poincaré map, and hence study of the occurrence of the period-doubling bifurcation and the Neimark-Sacker bifurcation.
- Use of the spectrum of Lyapunov exponents in the analysis of the scenario of period-doubling route to chaos. This study will be realized for only one case of the bifurcation diagram by varying only one parameter: the slope angle.

The remaining structure of this paper is as follows. A quick introduction of the compass-type bipedal robot and the mathematical model of its walking phases can be found in the second section. Then, by describing the Poincaré map approach in the third section for the localization of the period-1 fixed points, we will be interested in the hunting of a one-periodic bipedal walk of the compass robot using. The bifurcation diagrams and the analysis of various attractors in the fourth section are used to offer a study of the compass-type bipedal gait and to show the novel exhibited complex walking behaviors. The conclusion and a few upcoming projects are covered in the fifth and last Section.

PASSIVE DYNAMIC WALKING OF THE COMPASS BIPEDAL ROBOT

Geometric structure of the compass robot

Figure 1 shows a graphical presentation of the compass-gait biped robot, with Table 1 listing the significant parameters in the dynamics description. This biped robot is a type of rigid mechanical system with unilateral configuration space constraints (Chevallereau *et al.* 2009; Gritli *et al.* 2013; Westervelt *et al.* 2007).

The compass-type bipedal robot is made up of two legs that are exactly identical: a right leg and a left leg, as well as a frictionless hip that connects the two legs. The two legs are depicted as stiff bars without knees and ankles. The mass m of each leg is concentrated at a distance b from the mass m_h of the hip.

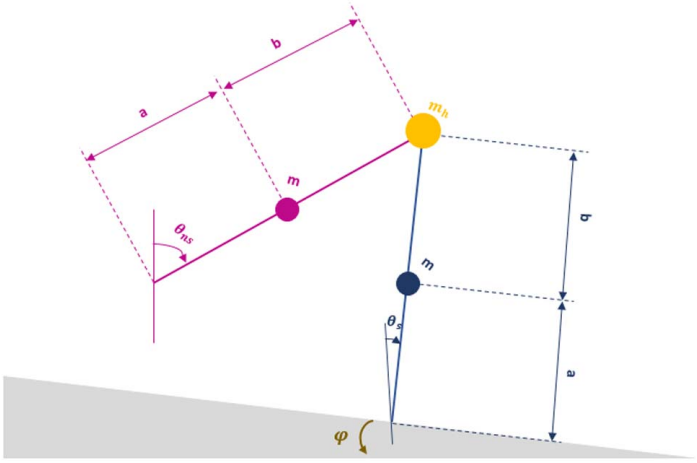

Figure 1 The passive compass bipedal robot walking down an inclined surface of angle φ. Here, θ_s and θ_{ns} stand respectively for the support angle of the support/stance leg, and the nonsupport angle of the swing leg. These angles are defined with regard to the vertical lines. Moreover, the positive angles are calculated in the counterclockwise direction.

Table 1 Significant parameters used in the dynamics description of the passive compass-type biped walker.

Notation	Value	Unit
a	0.5	m
b	0.5	m
l	1	m
m	5	Kg
m_h	10	Kg
g	9.8	ms^{-2}

The compass robot performs a passive walk without any external activity and relies solely on gravity for a suitable initial state and a corresponding slope φ. The passive walk of the compass robot contains two phases: a swing phase and a double-support phase or impact phase, which is a very fast transition phase. The compass-type bipedal robot can be modeled as a double pendulum in the first case with the stance leg stationary on the ground as a pivot and the other leg swinging above the ground as it walks down the hill. When the swing leg reaches the ground, the impulsive transition phase begins (and occurs instantaneously). As a result, the prior support leg departs the ground, and hence a new swing phase is developed.

We assume that the impact is totally inelastic and that there is no sliding at the point of contact between the leg and the ground (Gritli *et al.* 2015; Znegui *et al.* 2020a). In Figure 1 and in the sequel, θ_s is the angle of the support leg, whereas θ_{ns} is the angle of the swing leg. These two angles establish together the compass walk configuration. Note that positive angles are computed counterclockwise.

Modeling of the bipedal walk of the compass robot

The hybrid model of the compass-gait biped robot's passive dynamic walking combines of the nonlinear differential equation (3) for the swing phase and the nonlinear algebraic equation (7) for the impact phase.

Swing phase dynamics

Let $q = [\theta_{ns}\ \theta_s]^{\mathrm{T}}$ be the compass-gait biped robot's vector of generalized coordinates. According to (Znegui *et al.* 2020a), only one natural unilateral restriction is applied to this biped robot, namely

$$\mathcal{L}_1(q) = \theta_{ns} + \theta_s + 2\varphi \geq 0 \tag{1}$$

which corresponds to the distance between the hip of the swing leg and the ground. Thus, this constraint (1) represents the situation where and when the swing leg is upper the ground. This ensures that during bipedal walking, the unilateral restriction $\mathcal{L}_1 \geq 0$ is always satisfied.

The motion of the compass-gait biped robot can be defined as follows, by considering some basic assumptions (Gritli *et al.* 2015; Znegui *et al.* 2020a). Indeed, during the swing phase, we employ

the Euler-Lagrange method to determine the biped robot's dynamic model. The following is the expression for Euler-Lagrange equation for an uncontrolled robotic system, and therefore for the passive compass bipedal robot.

$$\frac{d}{dt}\frac{\partial \mathcal{L}(q,\dot{q})}{\partial \dot{q}} - \frac{\partial \mathcal{L}(q,\dot{q})}{\partial q} = 0 \tag{2}$$

From this previous expression (2), we get the following nonlinear differential equation:

$$\mathcal{M}(q)\ddot{q} + \mathcal{H}(q,\dot{q})\dot{q} + \mathcal{G}(q) = 0 \tag{3}$$

where $\mathcal{M}(q)$ is the inertia matrix:

$$\mathcal{M}(q) = \begin{bmatrix} mb^2 & -mlb\cos(\theta_s - \theta_{ns}) \\ -mlb\cos(\theta_s - \theta_{ns}) & (m+m_h)l^2 + ma^2 \end{bmatrix} \tag{4}$$

the matrix $\mathcal{H}(q,\dot{q})$ includes Coriolis and centrifugal forces:

$$\mathcal{H}(q,\dot{q}) = \begin{bmatrix} 0 & mbl\sin(\theta_s - \theta_{ns})\dot{\theta}_s \\ -mbl\sin(\theta_s - \theta_{ns})\dot{\theta}_{ns} & 0 \end{bmatrix} \tag{5}$$

and $\mathcal{G}(q)$ is the vector of gravitational torques:

$$\mathcal{G}(q) = \begin{bmatrix} -gmb\sin(\theta_{ns}) \\ g\left[(m+m_h)l + ma\right]\sin(\theta_s) \end{bmatrix} \tag{6}$$

It is worth noting that the control input, saying u, in the nonlinear dynamics (2) of the bipedal walking of the compass biped robot was not introduced, and then it is zero, $u = 0$. As a result, the compass bipedal robot is not controlled, and the swing phase, and consequently the complete bipedal walking, is hence entirely passive

Impact phase dynamics

The angular momentum conservation approach is used to determine the dynamics of the impact phase (Added *et al.* 2021b; Goswami *et al.* 1996, 1998). For this, we will use the two signs "+" and "−" that will be placed to the right of a variable to refer to the value of that variable, respectively, just after and just before the impact of the biped robot's swing leg with the ground.

The impact phase begins when the swing phase ends, which occurs when the compass walker's swing leg makes contact with the walking surface. When the swing leg encounters the walking surface, the angular momentum is conserved according to the following algebraic equation (Added *et al.* 2021b; Goswami *et al.* 1996, 1998):

$$\mathcal{Q}^+(q^+)\dot{q}^+ = \mathcal{Q}^-(q^+)\dot{q}^- \tag{7}$$

with $\dot{q}^+$ and $\dot{q}-$ are the angular velocities just after and just before the impact, where:

$$\mathcal{Q}^+(q) = \begin{bmatrix} mb(b - l\cos(\theta_s - \theta_{ns})) \\ mb^2 \\ ma^2 + m_h l^2 + ml(l - b\cos(\theta_s - \theta_{ns})) \\ -mlb\cos(\theta_s - \theta_{ns}) \end{bmatrix} \tag{8}$$

and

$$\mathcal{Q}^-(q) = \begin{bmatrix} -mab & l(m_h l + 2ma)\cos(\theta_s - \theta_{ns}) - mab \\ 0 & -mab \end{bmatrix} \tag{9}$$

Furthermore, when the impact with the ground occurs, a switching between the two legs happens. This situation is described by means of the following relation:

$$q^+ = \mathcal{R}q^- \tag{10}$$

where $\mathcal{R}$ is a constant matrix and is defined like so:

$$\mathcal{R} = \begin{bmatrix} 0 & 1 \\ 1 & 0 \end{bmatrix} \tag{11}$$

Relying on expressions of matrices $\mathcal{Q}^-(q)$ and $\mathcal{Q}^-(q)$, and by taking into consideration expressions (10) and (11), it is easy to demonstrate that the relation (7) can be recast as follows:

$$\dot{q}^+ = \left\{\mathcal{Q}^+(q^-)\right\}^{-1}\mathcal{Q}^-(q^-)\dot{q}^- \tag{12}$$

Impact conditions

According to the results in (Znegui *et al.* 2020a) and relying on the unilateral constraint (1), we can note the following condition:

$$\mathcal{L}_1(q) = 2\varphi + \theta_s + \theta_{ns} = 0 \tag{13}$$

which is the first impact condition and which reveals the case where the swing leg hits the walking surface.

Moreover, to ensure that the impact with the walking surface happens, we should add the following condition:

$$\mathcal{L}_2(q,\dot{q}) = \frac{d\mathcal{L}_1(q)}{dt} = \frac{\partial \mathcal{L}_1(q)}{\partial q}\dot{q} < 0 \tag{14}$$

which is the second impact condition revealing the case where the swing leg descends towards the walking surface.

In addition, in order to guarantee that the impact occurs after a complete swing phase, we add the following inequality constraint

$$\mathcal{L}_3(q) = \sin(\theta_{ns}) - \sin(\theta_s) > 0 \tag{15}$$

which is the third impact condition defining the case where the swing leg is opposite to (or it is in front of) the support leg.

Then, by arranging the previous expressions (13), (14) and (15), the impact conditions of the swing leg with the walking surface are defined by the following set:

$$\begin{cases} \mathcal{L}_1(q) = 2\varphi + \theta_{ns} + \theta_s = 0 \\ \mathcal{L}_2(q,\dot{q}) = \frac{\partial \mathcal{L}_1(q)}{\partial q}\dot{q} < 0 \\ \mathcal{L}_3(q) = \sin(\theta_{ns}) - \sin(\theta_s) > 0 \end{cases} \tag{16}$$

Complete dynamic model

The continuous dynamics presented in (3), the discrete dynamics presented in form of the two algebraic equations (12) and (10), and the set of impact conditions (16) form together the impulsive hybrid nonlinear dynamics of the passive dynamic walking model of the compass biped robot. Let $x = [q\ \dot{q}]^{\mathrm{T}}$ be the state vector.

Then, these previous expressions are grouped together to form the following impulsive hybrid nonlinear model:

$$\begin{cases} \dot{x} = f(x) \text{ if } x \in \Omega \\ x^{+} = h(x^{-}) \text{ if } x \in \Delta \end{cases} \tag{17}$$

where

$$\begin{cases} \Omega = \{x \in \mathbb{R}^{2n} : \mathcal{L}_1(x) > 0\} \\ \Delta = \{x \in \mathbb{R}^{2n} : \mathcal{L}_1(x) = 0; \mathcal{L}_2(x) < 0; \mathcal{L}_3(x) > 0\} \end{cases} \tag{18}$$

where here $n = 2$, and in (17),

$$f(x) = \begin{bmatrix} \dot{q} \\ -\mathcal{M}^{-1}(q)\left(\mathcal{H}(q,\dot{q})\dot{q} + \mathcal{G}(q)\right) \end{bmatrix} \tag{19a}$$

$$h(x) = \begin{bmatrix} \mathcal{R}q \\ \left\{\mathcal{Q}^{+}(q)\right\}^{-1}\mathcal{Q}^{-}(q)\dot{q} \end{bmatrix} \tag{19b}$$

Moreover, it is straightforward to show that the functions $\mathcal{L}_1(x)$ and $\mathcal{L}_2(x)$ are expressed like so:

$$\mathcal{L}_1(x) = \mathcal{C}_1 x + 2\varphi \tag{20a}$$

$$\mathcal{L}_2(x) = \mathcal{C}_2 x \tag{20b}$$

where

$$\mathcal{C}_1 = \begin{bmatrix} 1 & 1 & 0 & 0 \end{bmatrix} \tag{21a}$$

$$\mathcal{C}_2 = \begin{bmatrix} 0 & 0 & 1 & 1 \end{bmatrix} \tag{21b}$$

In addition, it is easy to show that the function $\mathcal{L}_2(x)$ is equivalent to:

$$\mathcal{L}_2(x) = \mathcal{C}_1 \dot{x} \tag{22}$$

IDENTIFICATION AND STABILITY OF THE ROBOT BIPED'S PERIODIC MOVEMENT

In this section, we will develop expressions of the fundamental solution matrix, the jump matrix, and the monodromy matrix, and use them to find a fixed point of the periodic movement of the compass-type bipedal robot.

Fundamental solution matrix

The first equation in the hybrid impulsive dynamic model (17) results from continuous behavior, whereas the second equation results from the discrete behavior. We consider first the nonlinear differential equation $\dot{x} = f(x)$, which proposes as a solution, which is expressed in terms of flow, defined like so:

$$x(t) = \phi(t, x_0) \tag{23}$$

and $x_0 = \phi(t_0, x_0)$, to be the initial condition.

It is simple to show that:

$$\dot{x} = f(x(t)) = \frac{dx(t)}{dt} = \frac{d\phi(t, x_0)}{dt} \tag{24}$$

Then, it is possible to write the following expressions:

$$\begin{cases} \dot{\phi}(t, x_0) = f(\phi(t, x_0)) \\ \phi(t_0, x_0) = x_0 \end{cases} \tag{25}$$

The derivative of these previous expressions in (25) with respect to the initial condition x_0, yields:

$$\begin{cases} \frac{\partial \dot{\phi}(t,x_0)}{\partial x_0} = \frac{\partial f(\phi(t,x_0))}{\partial x}\frac{\partial \phi(t,x_0)}{\partial x_0} \\ \frac{\partial \phi(t_0,x_0)}{\partial x_0} = \mathcal{I}_{2n} \end{cases} \tag{26}$$

where here and in the sequel $\mathcal{I}_{2n}$ stands for the identity matrix with dimension $(2n \times 2n)$.

We pose $\Phi(t, x_0)$ to be the fundamental solution matrix, which is expressed as follows:

$$\Phi(t, x_0) = \frac{\partial \phi(t, x_0)}{\partial x_0} \tag{27}$$

Then, the derivative of this matrix with respect to time leads to the following expression:

$$\dot{\Phi}(t, x_0) = \frac{\partial \dot{\phi}(t, x_0)}{\partial x_0} \tag{28}$$

Therefore, we can write the model (26) as follows:

$$\begin{cases} \dot{\Phi}(t, x_0) = \mathcal{J}(x)\Phi(t, x_0) \\ \Phi(t_0, x_0) = \mathcal{I}_{2n} \end{cases} \tag{29}$$

where $\mathcal{J}(x)$ is the Jacobian matrix of the nonlinear function $f(x)$, and is defined like so:

$$\mathcal{J}(x) = \frac{\partial f(\phi(t, x_0))}{\partial x} \tag{30}$$

The fundamental solution matrix $\Phi(t, x_0)$ is simple to calculate for continuous systems. However, its calculation is quite difficult for systems that are discontinuous or even show discontinuities, such as the impulsive hybrid dynamic systems as our biped robot's case. This problem to solve calls for the calculation of the jump matrix, as it will be explained in the next paragraph.

Jump matrix

The biped robots exhibit discontinuities as a result of the impact event in the Jacobian matrix during the transition of the state vector that results in a discontinuity or even a jump in the fundamental solution matrix $\Phi(t, x_0)$.

Let pose $\Phi^{+}(t, x_0)$ to be the fundamental solution matrix immediately after the impact, and $\Phi^{-}(t, x_0)$ to be the fundamental solution matrix immediately before the impact. The relation between $\Phi^{+}(t, x_0)$ and $\Phi^{-}(t, x_0)$ is obtained by means of the jump matrix $\mathcal{S}(x(\tau^{+}), x(\tau^{-}))$, as follows:

$$\Phi^{+}(t, x_0) = \mathcal{S}(x(\tau^{+}), x(\tau^{-}))\Phi^{-}(t, x_0) \tag{31}$$

Therefore, finding expression of the jump matrix $\mathcal{S}(x(\tau^{+}), x(\tau^{-}))$ is our goal in the next part.

Let posing for simplicity $x(\tau^{+}) = x^{+}$ and $x(\tau^{-}) = x^{-}$ with τ^{+} and τ^{-} are the moments right after and right before the impact. Moreover, we pose f^{+} to be the vector f immediately after the impact, and f^{-} to be the vector f immediately before the impact.

For simplicity, let us use in the next the following notations:

$$\begin{cases} \Phi^+ = \Phi(\tau^+, x_0) \\ \Phi^- = \Phi(\tau^-, x_0) \\ f^+ = f(x(\tau^+)) \\ f^- = f(x(\tau^-)) \end{cases} \tag{32}$$

As the flow $\phi(t, x_0)$ depends on t and x_0, it is then easy to write the following expression:

$$d\phi(t, x_0) = \frac{\partial \phi(t, x_0)}{\partial x_0} dx_0 + \frac{\partial \phi(t, x_0)}{\partial t} dt \tag{33}$$

Thus, we can write the relation:

$$\frac{d\phi(t, x_0)}{dx_0} = \frac{\partial \phi(t, x_0)}{\partial x_0} + \frac{\partial \phi(t, x_0)}{\partial t} \frac{dt}{dx_0} \tag{34}$$

Let us consider expressions (24) and (27), and posing $\tau_{x_0} = \frac{dt}{dx_0}$. Then, relation (34) can be reformulated as follows:

$$\frac{d\phi(t, x_0)}{dx_0} = \Phi(t, x_0) + f(\phi(t, x_0))\tau_{x_0} \tag{35}$$

Then, we can write for $t = \tau^-$ and $t = \tau^+$, the following expressions:

$$\begin{cases} \frac{dx(\tau^-)}{dx_0} = \Phi(\tau^-, x_0) + f(x(\tau^-))\tau_{x_0} \\ \\ \frac{dx(\tau^+)}{dx_0} = \Phi(\tau^+, x_0) + f(x(\tau^+))\tau_{x_0} \end{cases} \tag{36}$$

Then, using notation (32), expressions in (36) become:

$$\begin{cases} \frac{dx^-}{dx_0} = \Phi^- + f^-\tau_{x_0} \\ \\ \frac{dx^+}{dx_0} = \Phi^+ + f^+\tau_{x_0} \end{cases} \tag{37}$$

According to the second equation of the model (17), we have $x^+ = h(x^-)$. Then, it follows that:

$$\frac{dx^+}{dx_0} = \frac{dh(x^-)}{dx_0} = \frac{\partial h(x^-)}{\partial x^-} \frac{dx^-}{dx_0} \tag{38}$$

We pose $h_x^- = \frac{\partial h(x^-)}{\partial x^-}$. Then, relation (38) is rewritten like so:

$$\frac{dx^+}{dx_0} = h_x^- \frac{dx^-}{dx_0} \tag{39}$$

Therefore, based on the two results in (37), we can write from relation (39), the following expression:

$$\Phi^+ + f^+\tau_{x_0} = h_x^-(\Phi^- + f^-\tau_{x_0}) \tag{40}$$

According to the first impact condition in the set Δ in (18), we can write the following expression:

$$\frac{\partial \mathcal{L}_1(x^-)}{\partial x^-} \frac{dx^-}{dx_0} = 0 \tag{41}$$

Using expression (20a), and according to (41), it follows that:

$$\mathcal{C}_1 \frac{dx^-}{dx_0} = 0 \tag{42}$$

Therefore, relying on the first relation in (37), we obtain from the previous relation (42), the following expression:

$$\mathcal{C}_1(\Phi^- + f^-\tau_{x_0}) = 0 \tag{43}$$

Relying on the dynamics of the swing phase (24), we have:

$$\mathcal{C}_1 f^- = \mathcal{C}_1 \dot{x}^- \tag{44}$$

Moreover, relying on expression (22), it follows that (44) is recast like so:

$$\mathcal{C}_1 f^- = \mathcal{L}_2(x^-) \tag{45}$$

Then, according to the impact conditions describing the set Δ in (18), and then by considering the second condition $\mathcal{L}_2(x) < 0$, we obtain hence the following inequality:

$$\mathcal{C}_1 f^- < 0 \tag{46}$$

Accordingly, by taking into account this previous condition (46), and from the relation (43), expression of the quantity τ_{x_0} is defined as follows: :

$$\tau_{x_0} = \frac{-\mathcal{C}_1}{\mathcal{C}_1 f^-} \Phi^- \tag{47}$$

Hence, based on the equations (40) and (47), we can write the following relation:

$$\Phi^+ = (h_x^- - \frac{(h_x^- f^- - f^+)\mathcal{C}_1}{\mathcal{C}_1 f^-})\Phi^- \tag{48}$$

Therefore, compared to relation (31), the following expression describes the jump matrix:

$$\mathcal{S}(x^+, x^-) = h_x^- - \frac{(h_x^- f^- - f^+)\mathcal{C}_1}{\mathcal{C}_1 f^-} \tag{49}$$

Monodromy matrix

Let the set or hyperplan Δ describes our choice of the Poincaré section. Starting from the initial condition x_0 ($x_0 \in \Delta$), then the system trajectory will return to the Poincaré section Δ. The time required between two consecutive intersections with the Poincaré section is $T_r(x_0)$, which is called as the return time to the Poincaré section. For a one-periodic trajectory, the return time is the same as the period of the trajectory, and it defines the step period of the walking gait of the compass bipedal robot.

It is important to note that since the impact of the swing leg of the robot with the walking surface is instantaneous, then we can write the following relation:

$$T_r(x_0) = \tau^+ = \tau^- \tag{50}$$

For a 1-periodic trajectory and according to the equation (31), the monodromy matrix, namely Φ^+, is defined by the following relation:

$$\Phi^+ = \mathcal{S}(x^+, x^-)\Phi^- \tag{51}$$

where:

$$\Phi^- = \Phi(T_r(x_0), x_0) = \left. \frac{\partial f(\phi(t, x_0))}{\partial \phi(t, x_0)} \right|_{t=\tau^-} \tag{52}$$

Notice that $\Phi(T_r(x_0), x_0)$ is the fundamental solution matrix $\Phi(t, x_0)$, which is the solution of the differential system (29), and evaluated at the first return time $T_r(x_0)$. Then, we stress that the fundamental solution matrix $\Phi(t, x_0)$ depends on the values of

the state vector x just before (x^-) and just after (x^+) the impact event. These two states x^- and x^+ are completely different, and hence they will give us two different values of the fundamental solution matrix $\Phi(t, x_0)$ at the impact that are related via relation (48). Therefore, this sudden and non-continuous change in values of the fundamental solution matrix causes a discontinuity.

It is worth to mention that the search for the one-periodic walk for the compass-type biped robot lies in the search for a one-periodic fixed point of the period-1 limit cycle.

Finding a period-1 fixed point

The period-1 fixed point is the solution of the following equation:

$$\mathcal{F}(x_0) = \mathcal{P}(x_0) - x_0 = \phi(T_r(x_0), x_0) - x_0 = 0 \tag{53}$$

To determine the solutions of this equation (53), we use the numerical Newton-Raphson algorithm. We choose an initial estimate of x_0 as an initial condition, then we iterate the Poincaré map only once to find the flow $\phi(\tau^+, x_0)$.

Algorithm

The search algorithm for a period-1 fixed point is based on the following iterative scheme:

$$x_0^{k+1} = x_0^k - \left\{\mathcal{DF}(x_0^k)\right\}^{-1} \mathcal{F}(x_0^k) \tag{54}$$

where $\mathcal{DF}(x_0^k)$ is the Jacobian of the function $\mathcal{F}$ presented in the equation (53).

The algorithm stops when the norm of $\mathcal{F}(x_0^k)$ will be lower than a certain fixed threshold.

Expression of the Jacobian matrix $\mathcal{DF}(x_0)$

To solve the equation (54), the Jacobian matrix $\mathcal{DF}(x_0^k)$ must be first calculated. This matrix is defined by the following expression:

$$\mathcal{DF}(x_0) = \frac{d\mathcal{F}(x_0)}{dx_0} \tag{55}$$

Then, using relation (53), we have:

$$\mathcal{DF}(x_0) = \frac{d}{dx_0}(\phi(T_r(x_0), x_0) - x_0) \tag{56}$$

Thus, we obtain the following expression:

$$\mathcal{DF}(x_0) = \frac{d\phi(T_r(x_0), x_0)}{dx_0} - \mathcal{I}_{2n} \tag{57}$$

Expression of the quantity $\frac{d}{dx_0}\phi(T_\tau(x_0), x_0)$

Relying on expression (33), we can write the following relation:

$$d\phi(T_r(x_0), x_0) = \frac{\partial\phi(T_r(x_0), x_0)}{\partial x_0} dx_0 + \frac{\partial\phi(T_r(x_0), x_0)}{\partial T_r(x_0)} dT_r(x_0) \tag{58}$$

Then, we obtain the following expression of the quantity $\frac{d\phi(T_\tau(x_0), x_0)}{dx_0}$:

$$\frac{d\phi(T_\tau(x_0), x_0)}{dx_0} = \frac{\partial\phi(T_\tau(x_0), x_0)}{\partial x_0} + \frac{\partial\phi(T_\tau(x_0), x_0)}{\partial T_\tau(x_0)} \frac{dT_r(x_0)}{dx_0} \tag{59}$$

The previous expression can be rewritten like so:

$$\frac{d\phi(T_\tau(x_0), x_0)}{dx_0} = \Phi(T_\tau(x_0), x_0) + f(x(T_r(x_0))) \frac{dT_r(x_0)}{dx_0} \tag{60}$$

where $\Phi(T_\tau(x_0), x_0)$ is the fundamental solution matrix $\Phi(t, x_0)$ evaluated at the return time $T_\tau(x_0) = \tau^+$, and then $\Phi(T_\tau(x_0), x_0) = \Phi^+$. Moreover, we have $f(x(T_r(x_0))) = f(x(\tau^+)) = f^+$.

Then, the equation (57) becomes:

$$\mathcal{DF}(x_0) = \Phi(T_\tau(x_0), x_0) + f(x(T_\tau(x_0))) \frac{dT_\tau(x_0)}{dx_0} - \mathcal{I}_{2n} \tag{61}$$

The only unknown in this expression (61) is the quantity $\frac{dT_r(x_0)}{dx_0}$, which will be determined in the next section.

Expression of the quantity $\frac{dT_r(x_0)}{dx_0}$

Let us reconsider the two first impact conditions in the impact set Δ defined in (18):

$$\mathcal{L}_1(x) = \mathcal{C}_1 x + 2\varphi = 0 \tag{62a}$$
$$\mathcal{L}_2(x) = \mathcal{C}_2 x < 0 \tag{62b}$$

For a period-1 fixed point, we should have $x_0 = \phi(T_r(x_0), x_0)$. Then, the two impact conditions in (62a) and (62b) are recast as follows:

$$\mathcal{L}_1(\phi(T_r(x_0), x_0)) = \mathcal{C}_1\phi(T_r(x_0), x_0) + 2\varphi = 0 \tag{63a}$$
$$\mathcal{L}_2(\phi(T_r(x_0), x_0)) = \mathcal{C}_2\phi(T_r(x_0), x_0) < 0 \tag{63b}$$

The derivative of the first constraint (63a) with respect to x_0 is as follows:

$$\frac{d\mathcal{L}_1(\phi(T_r(x_0), x_0))}{dx_0} = \frac{\partial\mathcal{L}_1(\phi(T_r(x_0), x_0))}{\partial x_0} + \frac{\partial\mathcal{L}_1(\phi(T_r(x_0), x_0))}{\partial T_r(x_0)} \frac{dT_r(x_0)}{dx_0} = 0 \tag{64}$$

Moreover, we can write the following relations:

$$\frac{\partial\mathcal{L}_1(\phi(T_r(x_0), x_0))}{\partial x_0} = \frac{\partial\mathcal{L}_1(\phi(T_r(x_0), x_0))}{\partial\phi(T_r(x_0), x_0)} \frac{\partial\phi(T_r(x_0), x_0)}{\partial x_0} \tag{65a}$$
$$\frac{\partial\mathcal{L}_1(\phi(T_r(x_0), x_0))}{\partial T_r(x_0)} = \frac{\partial\mathcal{L}_1(\phi(T_r(x_0), x_0))}{\partial\phi(T_r(x_0), x_0)} \frac{\partial\phi(T_r(x_0), x_0)}{\partial T_r(x_0)} \tag{65b}$$

According to expression (63a), we obtain:

$$\frac{\partial\mathcal{L}_1(\phi(T_r(x_0), x_0))}{\partial\phi(T_r(x_0), x_0)} = \mathcal{C}_1 \tag{66}$$

Then, the two expressions (65a) and (65a) become:

$$\frac{\partial\mathcal{L}_1(\phi(T_r(x_0), x_0))}{\partial x_0} = \mathcal{C}_1 \frac{\partial\phi(T_r(x_0), x_0)}{\partial x_0} \tag{67a}$$
$$\frac{\partial\mathcal{L}_1(\phi(T_r(x_0), x_0))}{\partial T_r(x_0)} = \mathcal{C}_1 \frac{\partial\phi(T_r(x_0), x_0)}{\partial T_r(x_0)} \tag{67b}$$

Then, relation (64) is recast as follows:

$$\mathcal{C}_1 \frac{\partial\phi(T_r(x_0), x_0)}{\partial x_0} + \mathcal{C}_1 \frac{\partial\phi(T_r(x_0), x_0)}{\partial T_r(x_0)} \frac{dT_r(x_0)}{dx_0} = 0 \tag{68}$$

This expression (68) is rewritten like so:

$$\mathcal{C}_1\Phi(T_r(x_0), x_0) + \mathcal{C}_1 f(x(T_r(x_0))) \frac{dT_r(x_0)}{dx_0} = 0 \tag{69}$$

Accordingly, as $\mathcal{C}_1 f(x(T_r(x_0))) = \mathcal{C}_1 f^-$, and based on the condition (46), we can obtain expression of the quantity $\frac{dT_\tau(x_0)}{dx_0}$ as follows:

$$\frac{dT_\tau(x_0)}{dx_0} = \frac{-\mathcal{C}_1}{\mathcal{C}_1 f(x(T_\tau(x_0)))} \Phi(T_\tau(x_0), x_0) \tag{70}$$

We substitute expression (70) into the equation (61), then we get expression of the matrix $\mathcal{DF}(x_0)$ as follows:

$$\mathcal{DF}(x_0) = (\mathcal{I}_{2n} - \frac{f(x(T_r(x_0)))\mathcal{C}_1}{\mathcal{C}_1 f(x(T_r(x_0)))})\Phi(T_r(x_0), x_0) - \mathcal{I}_{2n} \quad (71)$$

or under its simplified version

$$\mathcal{DF}(x_0) = (\mathcal{I}_{2n} - \frac{f^-\mathcal{C}_1}{\mathcal{C}_1 f^-})\Phi^+ - \mathcal{I}_{2n} \quad (72)$$

It is important to show that the Jacobian matrix of the Poincaré map $\mathcal{P}$ is defined as follows:

$$\mathcal{DP}(x_0) = (\mathcal{I}_{2n} - \frac{f^-\mathcal{C}_1}{\mathcal{C}_1 f^-})\Phi^+ \quad (73)$$

ANALYSIS OF THE COMPASS-TYPE BIPEDAL ROBOT'S PASSIVE WALK

The impulsive hybrid nonlinear system describing the compass-gait biped walker's walking dynamics is thought to be difficult to analyze and can produce complex appealing behaviors. The cascade of repeated period-doubling bifurcations and their consequent route to chaos is the most prevalent behavior revealed in the passive dynamic walking of the compass-gait bipedal walker as it moves down the walking surface. All circumstances must be taken into consideration in order to more accurately resemble humans especially the physically handicapped which are more and more apparent. When the knee is not in the middle of the leg, for instance, the length of the shank and the thigh are not equal, which shifts the center of gravity from its typical location. We shall analyze this situation by walking on various slope angles of surfaces. To achieve this, we will use bifurcation diagrams to demonstrate novel exhibited behaviors by changing two parameters: the length a of the lower-half segment of the two legs (see Figure 1) and the slope φ of the inclined walking surface.

Analysis via bifurcation diagrams

Complex exhibited behavior with respect to the slope angle φ

In this section, we adjust the slope angle φ of the walking surface and we calculate the new walking step of the compass biped robot while maintaining constant the other geometrical characteristic parameters listed in Table 1.

A conventional bifurcation diagram is shown in Figure 2(a) that illustrates the period-doubling scenario exhibited for the parameter $a = 0.5$. The diagram starts with a 1-periodic behavior for φ values between 0° and 4.385°, then changes to a 2-periodic behavior as indicated by the two red arrows, then to a 4-periodic gait, to a 8-periodic gait, and so on, until reaching chaos, which is framed in green.

Similarly, and by fixing another value of the parameter $a = 0.87$, we obtain the bifurcation diagram in Figure 2(b). This diagram shows a period-doubling phenomenon as a route to chaos. Such scenario begins at the value $\varphi = 7.552^\circ$ and doubles until chaos, and ends with the fall of the bipedal robot (for $\varphi \approx 11^\circ$). The difference between the two first diagrams (Figure 2(a) and Figure 2(b)) is that for $a = 0.87$, the biped robot's passive gait returns to another periodic behavior to start another period-doubling scenario to chaos instead of falling after the initial formation of chaos, as it has been occurred in Figure 2(a). This new period-doubling scenario will be finished around the value of $\varphi = 9.864^\circ$. This phenomenon reveals the appearance of periodicity window that was born within the chaotic regime contrary to the bifurcation diagram in Figure 2(a).

Furthermore, for the parameter $a = 0.881$, we observe from Figure 2(c) that the band of φ-values in which chaos occurs is quite narrow, which is another feature that is revealed. Such band occurs between $\varphi = 10.79$ and $\varphi = 10.93$. That is to say, as soon as chaos sets in, the robot falls fairly quickly.

Figure 2(d) illustrates a different kind of bifurcation scenario and then another phenomenon. It is found that the period doubles from 1-periodic to 2-periodic to 4-periodic up to 8-periodic behavior. After that, a remerging-period bifurcation is developed before going back to one-periodic behavior. The bipedal robot falls down at the point $\varphi = 12.21^\circ$, shortly after the Neimark-Sacker bifurcation (NSB), which will be clearer in the next diagram.

In Figure 2(e), and for the parameter $a = 0.895$, the period-doubling schema has been changed and reduced to a single period-doubling bifurcation follows by another one. Thus, the 1-periodic gait is bifurcated into a 2-periodic gait and it returns again to the 1-periodic gait via the period-doubling bifurcation. Thus, by increasing the bifurcation parameter φ, a Neimark-Sacker bifurcation is hence produced giving rise to the formation of a quasi-periodic behavior. Further analysis of this Neimark-Sacker bifurcation will be realized in the sequel.

In the bifurcation diagram of Figure 2(f) depicted for $a = 0.95$, only the period-1 passive gait was observed. Moreover, the single and attractive element in this bifurcation diagram is the zoomed-out red-circled part that reveals occurrence of the Neimark-Sacker bifurcation. As in Figure 2(e), this bifurcation demonstrates how, for $\varphi = 7.7^\circ$, the behavior changes from a 1-periodic to quasi-periodic. The quasi-periodic behavior occurs in a very small interval of slopes, which is not clear in the bifurcation diagram of Figure 2(f), compared to that in Figure 2(e).

Complex exhibited behavior with respect to the lower-leg segment length a

In this part, we maintain the other geometrical properties stated in the Table 1 while adjusting the lower-leg segment length a and calculating the new walking stride of the compass biped robot. The simulation results for different values of the bifurcation parameter a are illustrated in Figure 3.

It can be reported from the bifurcation diagrams in Figure 3 that every minor change in the value of the parameter a can result in a significant change in the walking behavior of the compass robot. Moreover, in all these bifurcation diagrams in Figure 3, the passive gaits exhibit a 1-periodic behavior for the values of a greater than the value 0.5°.

A single period-doubling bifurcation from 1-periodic gait to 2-periodic gait is seen in Figure 3(a) for $\varphi = 0.1^\circ$. In the other diagrams, it gradually alters.

Figure 3(b) shows the exhibited phenomenon for $\varphi = 0.54^\circ$ and demonstrates how the robot's behavior or step period changes from 2-periodic to 4-periodic as a result of the emergence of tiny bubbles.

For $\varphi = 0.56^\circ$ in Figure 3(c), the periodicity is clearly obvious. The bipedal robot falls down as a result of the Neimark-Sacker bifurcation at the end of this period doubling.

Figure 3(d) depicts further bubbles that form within these final ones. In the center of these bubbles, we notice a 16-periodic behavior. It is therefore pretty obvious that within these bubbles and by raising the value of φ, we find a period doubling that can lead to chaos, as shown in Figure 3(e) for $\varphi = 0.6^\circ$, followed by a remerging-period bifurcation to go back to 2-periodic, which finishes at the Neimark-Sacker bifurcation. A classical period-doubling bifurcation from 1-periodic gait to chaotic one can be seen in Figure 3(f) for the parameter $\varphi = 0.61^\circ$.

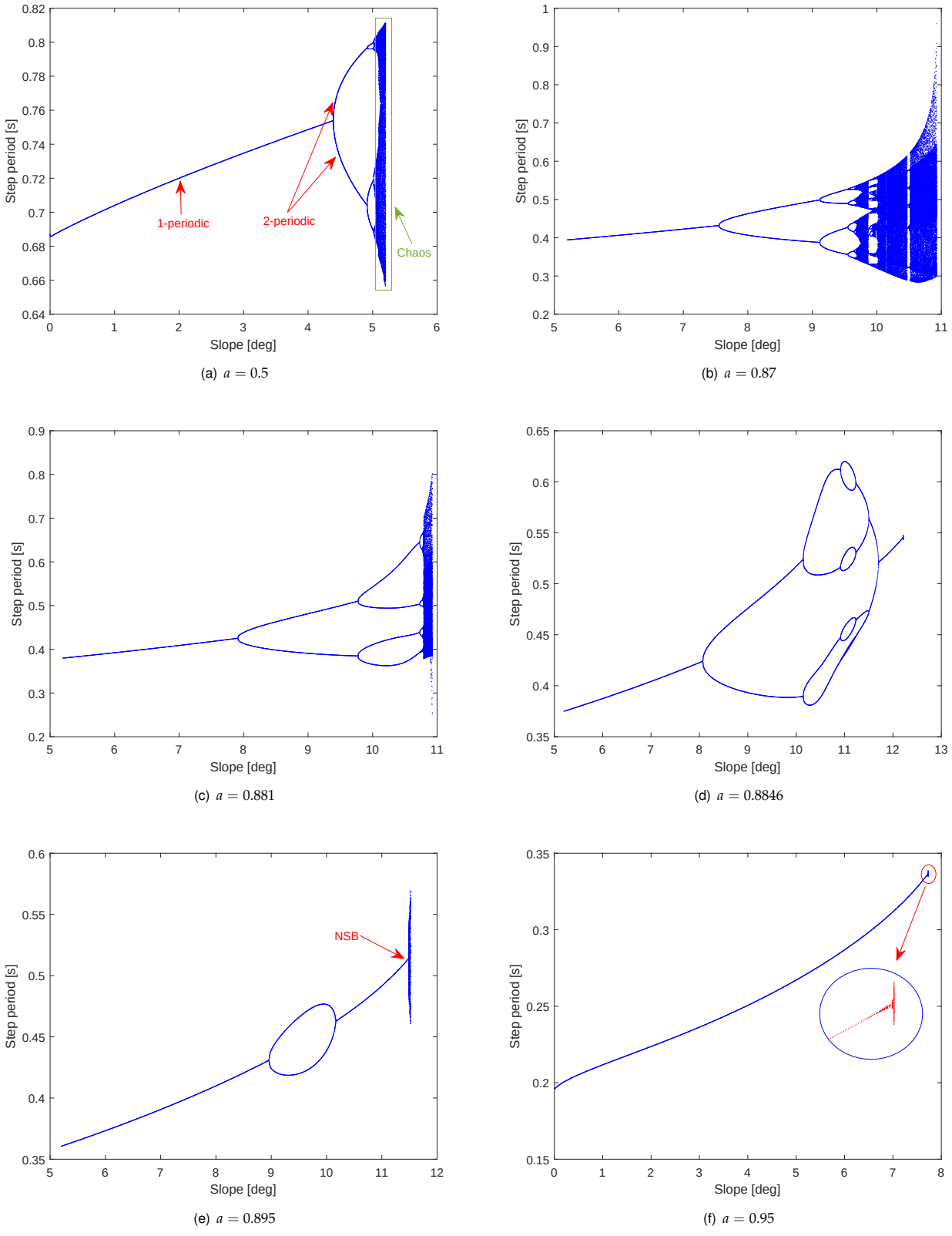

(a) $a = 0.5$

(b) $a = 0.87$

(c) $a = 0.881$

(d) $a = 0.8846$

(e) $a = 0.895$

(f) $a = 0.95$

Figure 2 Bifurcation diagrams of the step period of the bipedal's walking plotted by varying the slope angle φ for (a) $a = 0.5$ showing the classical period-doubling bifurcation (PDB) route from 1-periodic to chaos, (b) for $a = 0.87$ showing the PDB with a large part of chaos containing bifurcation/periodicity windows, (c) for $a = 0.881$ showing also the PDB with a compass robot that falls down quickly after chaos, (d) for $a = 0.8864$ showing succession of the PDB and the remerging-period bifurcation followed by the Neimark-Sacker bifurcation (NSB), (e) for $a = 0.895$ showing a bubble that is the result of the 1-PDB and the 1-remerging-period bifurcation also followed by the NSB in a wide interval, and (f) for $a = 0.95$ showing the NSB.

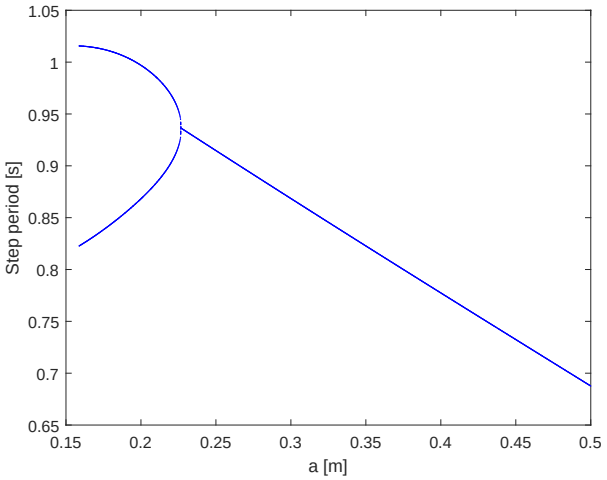

(a) $\varphi = 0.1^\circ$

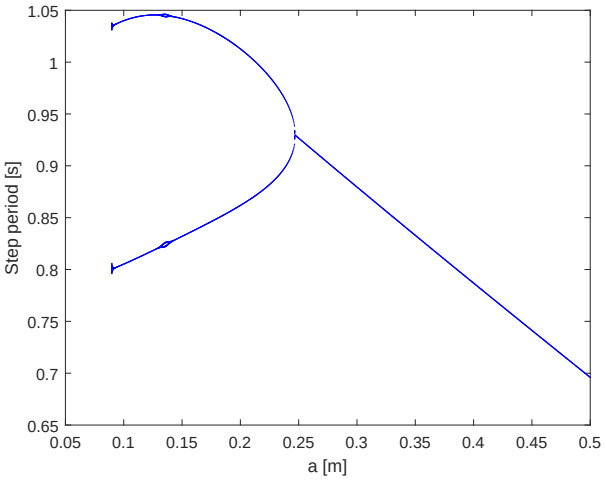

(b) $\varphi = 0.54^\circ$

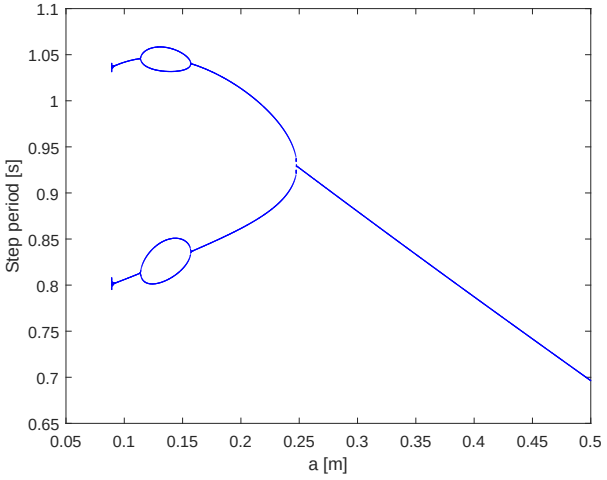

(c) $\varphi = 0.56^\circ$

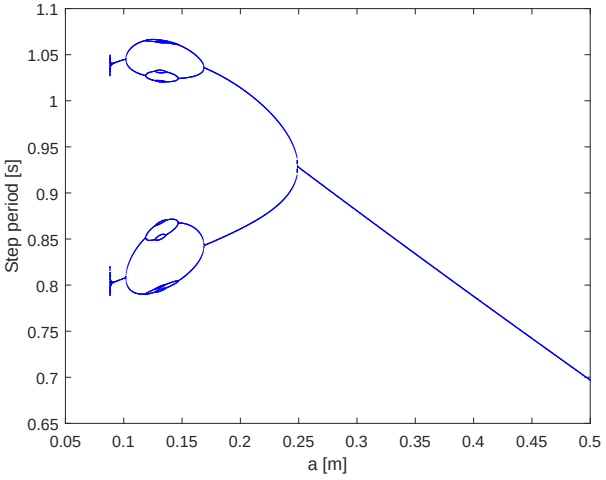

(d) $\varphi = 0.59^\circ$

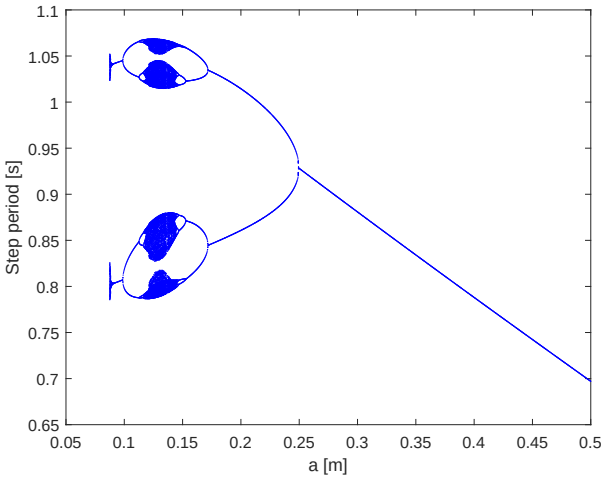

(e) $\varphi = 0.6^\circ$

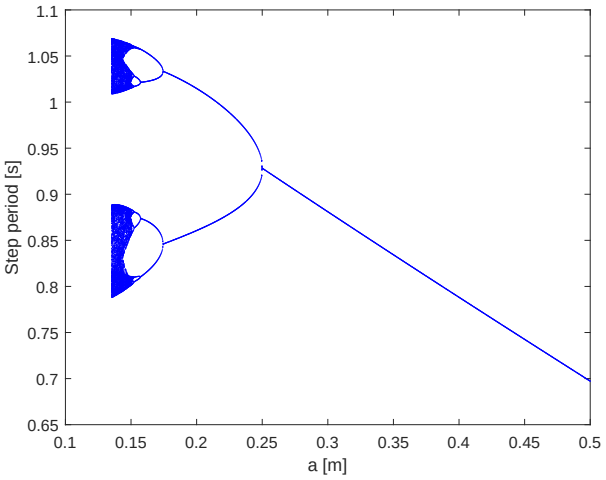

(f) $\varphi = 0.61^\circ$

Figure 3 Bifurcation diagrams plotted by varying the lower-leg segment length a for (a) $\varphi = 0.1^\circ$ showing the 1-PDB, (b) for $\varphi = 0.54^\circ$, (c) for $\varphi = 0.56^\circ$, (d) for $\varphi = 0.59^\circ$, (e) for $\varphi = 0.6^\circ$ showing the succession of the PDB route to chaos and the remerging-period bifurcation from chaos followed by the NSB, and (f) for $\varphi = 0.61^\circ$ showing the PDB ended by the fall of the bipedal robot.

Remark 1 *In addition to the step period, there are other descriptors of the passive dynamic walking of bipedal robots such as the step length, the average speed of each walking step, the mechanical energy, the angular positions and angular velocities just after/before the impact event with the ground (Goswami et al. 1996, 1998). The study of the apex can refer to the complexity of the bipedal walking as in (Gupta and Kumar 2017; Xie et al. 2020). The study of the apex consists in seeking the maximum position of the hip that can be reached by the biped robot while walking. Thus, such maximum position is such that the vertical speed of the hip is zero.*

It is straightforward to find that the vertical position of the hip of the compass robot is defined by the following expression:

$$z_{hip} = l\cos(\theta_s) \tag{74}$$

Thus, the vertical speed of the hip is defined as follows:

$$\dot{z}_{hip} = -l\dot{\theta}_s \sin(\theta_s) \tag{75}$$

Therefore, to obtain a zero vertical speed of the hip, we should have $\dot{z}_{hip} = 0$*, and then we should obtain:*

$$\dot{\theta}_s \sin(\theta_s) = 0 \tag{76}$$

Obviously, either $\sin(\theta_s) = 0$ *or* $\dot{\theta}_s = 0$ *to verify equality constraint (76). Relying on the structure of the compass robot, only the angular position* $\theta_s = 0$ *is realizable. Moreover, the angular position of the stance leg is always in variation as seen in the attractors in Figure 9. It can be seen that the angular velocity of the stance leg is always negative (*$\dot{\theta}_s < 0$*). Therefore, the angular velocity of the stance leg* $\dot{\theta}_s$ *cannot be 0. Hence, the only feasible solution that verifies the equality condition (76) is:*

$$\theta_s = 0 \tag{77}$$

Then, we should look for the descriptors of the passive bipedal walking of the compass robot such that the condition (77) is satisfied. Actually, this equality constraint (77) defines a new Poincaré section on which we look for new observation of the dynamics of the bipedal walking of the compass robot. Figure 4 shows two bifurcation diagrams revealing the complex behavior of the passive bipedal walking of the compass robot at its apex position while varying the slope angle φ *and with* $a = 0.5$*. Figure 4(a) reveals the walking time, whereas Figure 4(b) illustrates the angular velocity of the stance leg at the apex position. Notice that for* $a = 0.5$*, the bifurcation diagram at the impact of the swing leg with the ground was given by Figure 2(a) with* $a = 0.5$*. It is clear that by comparing the bifurcation diagram in Figure 2(a) with that in Figure 4(a), the behavior is almost similar, where the classical period-doubling route to chaos was revealed. However, in Figure 4(a), the (median) walking time at the apex position is almost constant while varying the slope angle* φ*. In contrast, in Figure 2(a), the (median) step period increases with respect to the increase of the slope* φ*. This result shows that the swing phase that happens just after the apex becomes longer by increasing the slope parameter* φ*.*

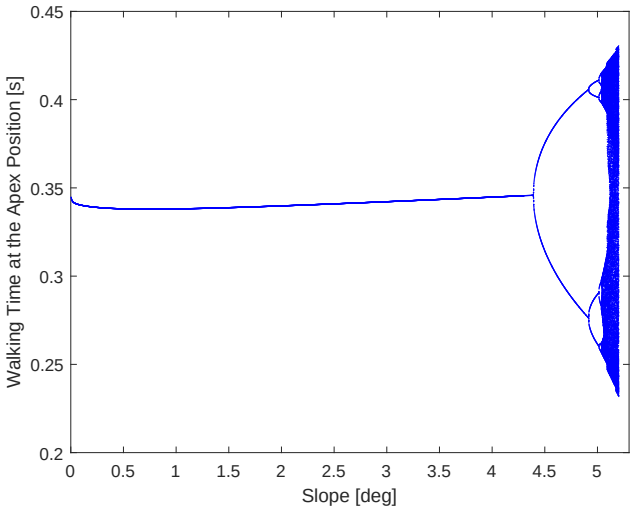

(a) $a = 0.82$

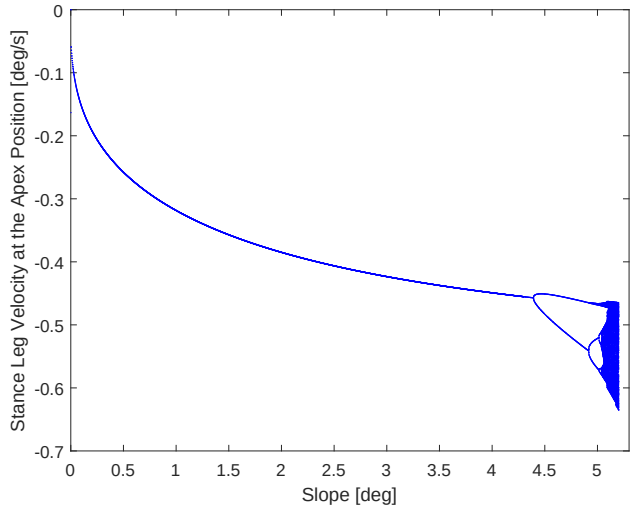

(b) $a = 0.83$

Figure 4 Bifurcation diagrams revealing the behavior of the bipedal walking at the apex position of the compass robot: (a) the walking time, and (b) the angular velocity of the stance leg. Here, the bifurcation parameter is the slope angle φ and the other parameter a was fixed to the nominal value $a = 0.5$.

Analysis of complex and strange behaviors

Figure 5, which is an addition to the previous section's illustrations, reveals a different phenomenon. By comparing the two figures, it seems that they are identical, with the exception that in Figure 5(a), there is some missing component that was present in Figure 5(b) and that was disappeared at the value $\varphi = 9.008°$ in Figure 5(a).

The same previous observation can be seen in Figure 6 by considering the bifurcation parameter a. For $\varphi = 0.605°$, the passive gait shows a classical period-doubling route to chaos, as seen in Figure 6(a). This exhibited behavior ends at the value $a = 0.133$, which provokes the fall of the bipedal robot. However, by slightly decreasing the value of the slope angle to $\varphi = 0.604°$, we see a completely different phenomenon. Indeed, a period-doubling route to chaos was first generated by decreasing the bifurcation parameter a. By decreasing further a, an inverse period-doubling scenario from chaos to a period-2 gait was observed. This period-2 gait was disappeared at the value $a = 0.0877$.

Accordingly, a very slight change in the value of the slope φ induces an almost different bifurcation diagram by varying the parameter a. As in Figure 5 by moving from the value $a = 0.83$ to $a = 0.82$ and where a complete part of the bifurcation diagram was disappeared, in Figure 6 and by changing/increasing the value of the slope from $\varphi = 0.604°$ to $\varphi = 0.604°$, a complete part of the bifurcation diagram was also disappeared without any explanation.

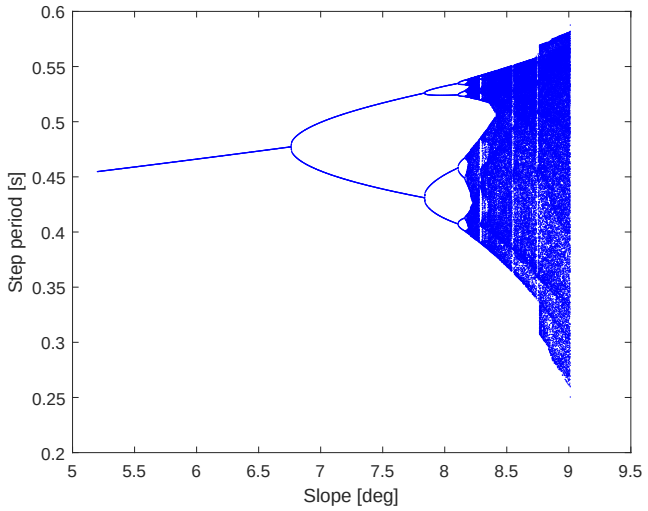

(a) $a = 0.82$

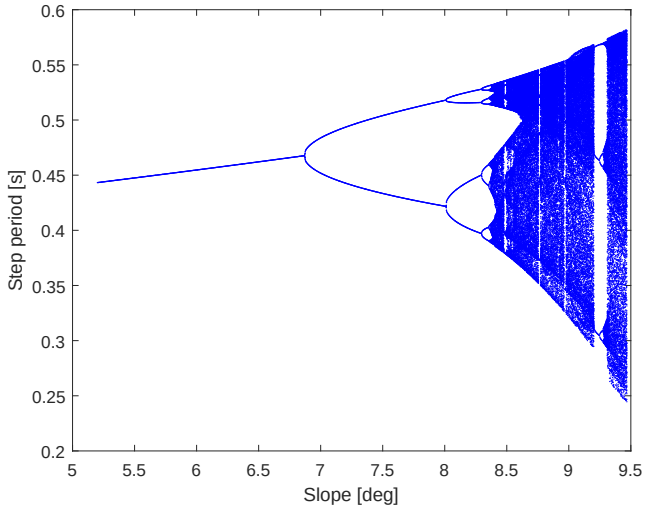

(b) $a = 0.83$

Figure 5 Bifurcation diagrams of the step period plotted by varying the slope angle φ for (a) $a = 0.82$ and (b) $a = 0.83$, showing the large variation of the step period (walking behavior) with respect to a tiny variation of the parameter a, which confirms the chaotic/strange nature of the passive walking dynamics of the compass bipedal robot. A large periodicity window appears in the bifurcation diagram (b). Such window and the result behavior leading to the formation of chaos was not observed in the bifurcation diagram (a).

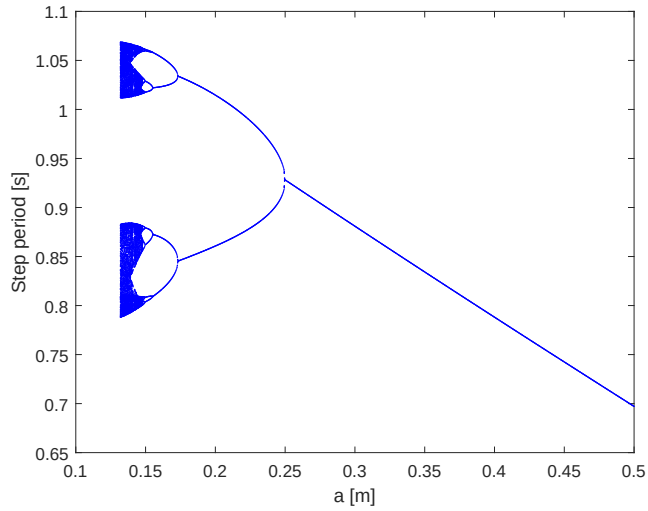

(a) $\varphi = 0.605^\circ$

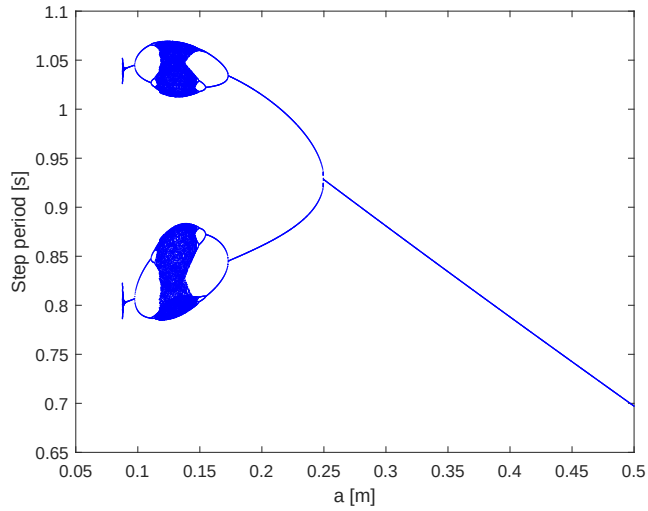

(b) $\varphi = 0.604^\circ$

Figure 6 Bifurcation diagrams of the step period plotted by varying the parameter a for (a) $\varphi = 0.605^\circ$ and (b) $\varphi = 0.604^\circ$, showing the sudden disappearance of some region/part of steady gaits of the passive compass robot. Such disappeared part is that located at the left side of the bifurcation diagram revealing the period-remerging scenario from chaos to the period-2 gait to the quasi-periodic gait. Such abrupt disappearance of these phenomena was occurred under a small variation of the slope angle φ.

Analysis via the characteristic multipliers

In addition to the stable solutions shown in the bifurcation diagram of Figure 5(a), we also presented the unstable solutions in the same plot as seen in Figure 7(a). These unstable solutions were represented by a dotted magenta line with the designation p1-ULC, which began at the first period-doubling bifurcation at the value of $\varphi = 6.771^\circ$. This shaky solution comes to an end at or near the value of $\varphi = 18^\circ$. The persistence of this unstable solution long after the biped robot has fallen suggests the presence of additional isolated components, which are depicted in Figure 5(b).

Figure 7(b) shows the evolution of the eigenvalues of the Jacobian matrix of the Poincaré map calculated via expression (71). This diagram in Figure 7(b) provides a strong support for this previous observation. We can see that the green eigenvalue takes values above the value 1, which is shown by a dotted line in black. Note that the value $\varphi = 6.771^\circ$ marks the birth of the bifurcation. This eigenvalue continues to vary even after the end of chaos at the value of $\varphi = 9.01^\circ$, which reveals the continued appearance of solutions but that is evident that they are unstable. According to the stability condition, as long as the characteristic multipliers lie inside the unit circle, the periodic solution is asymptotically stable. As φ is increased, a real characteristic multiplier moves out of the

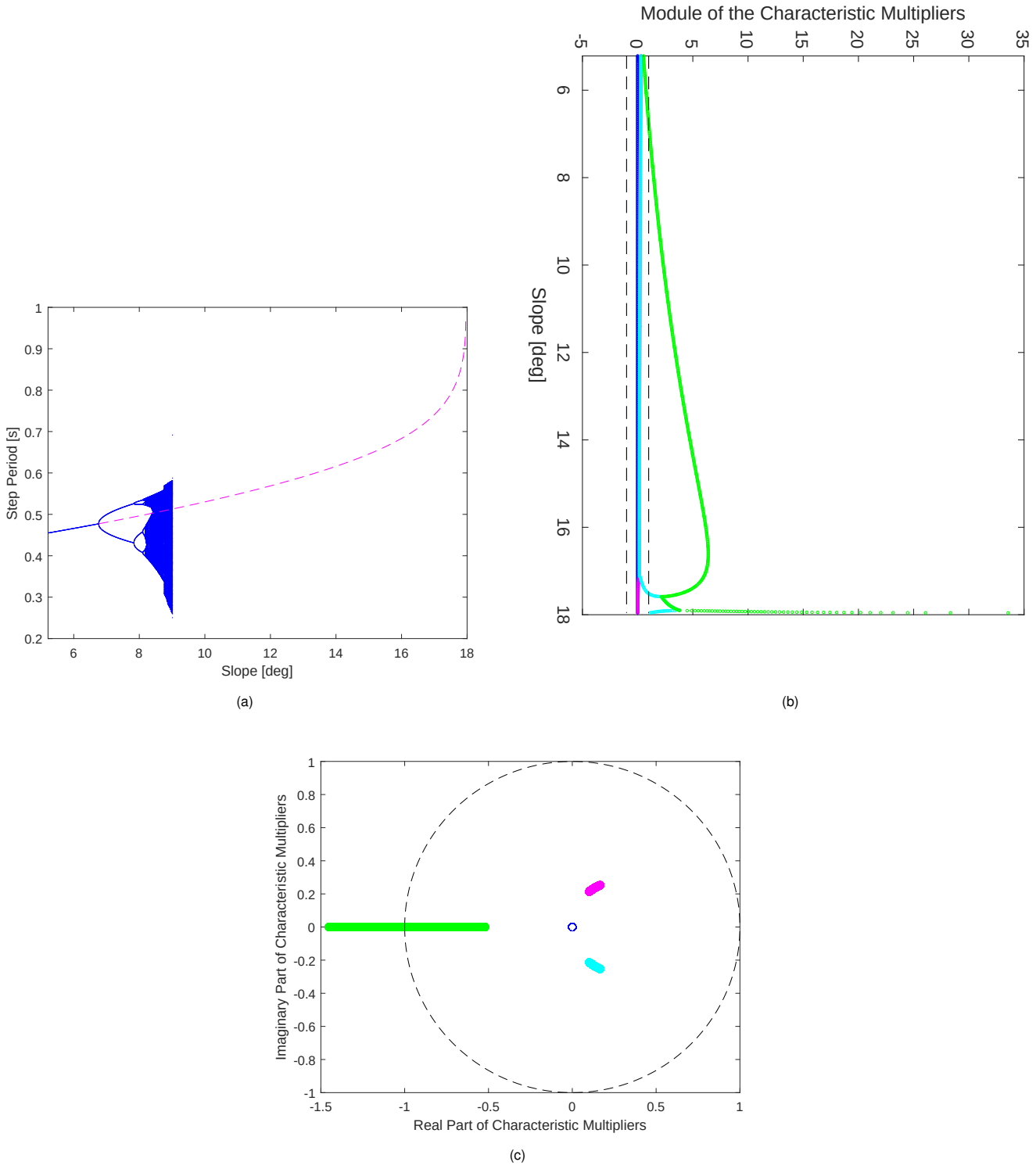

Figure 7 (a) Bifurcation diagram of the step period for $a = 0.82$ by varying the slope angle φ showing the period-1 unstable limit cycle (marked as p1-ULC), (b) Variation of the module of the eigenvalues of the Jacobian matrix of the Poincaré map, and (c) Variation of the loci of the characteristic multipliers with respect to the unit circle, as varying the slope angle φ for the fixed parameter $a = 0.82$.

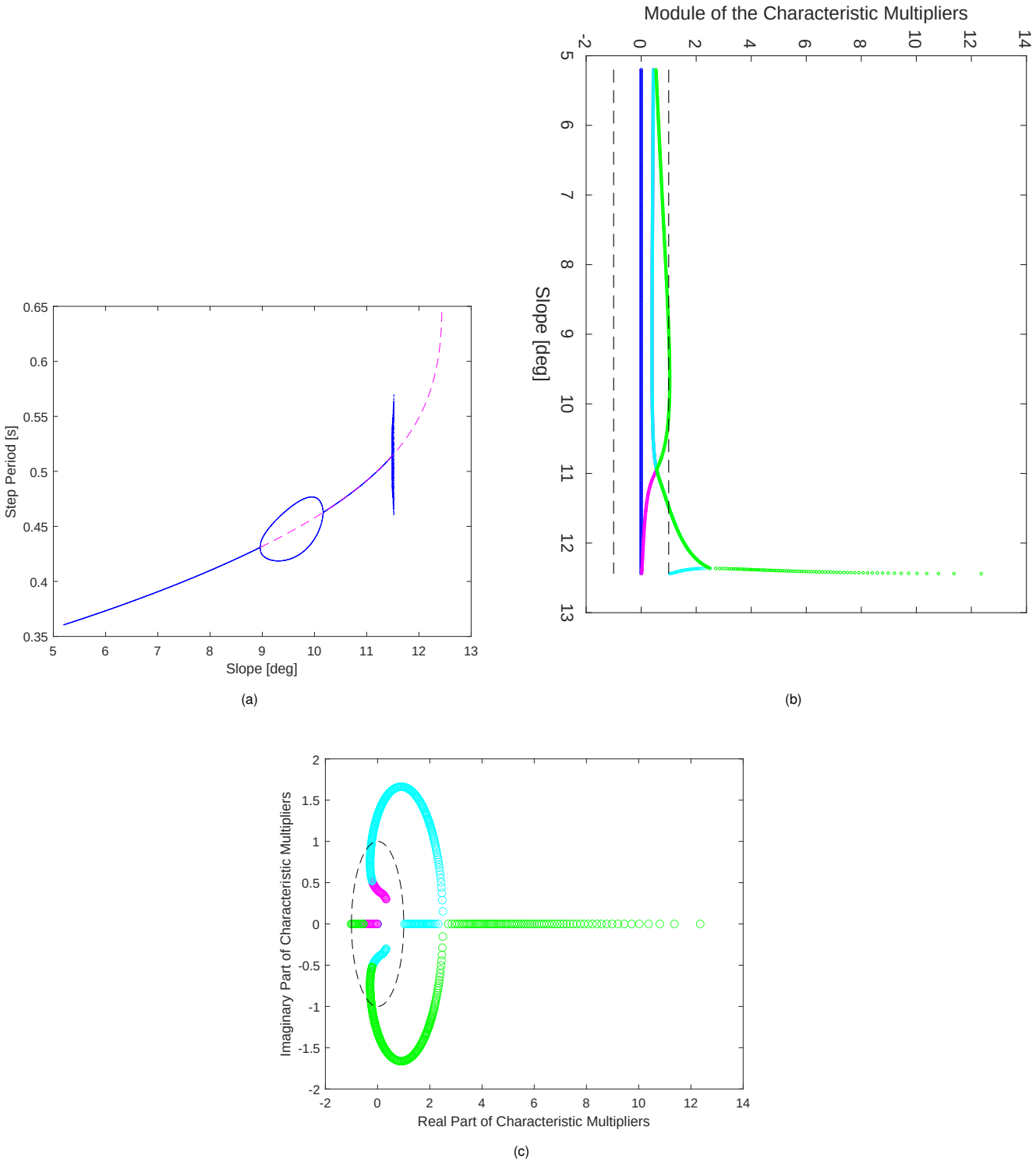

Figure 8 (a) Bifurcation diagram of the step period for the fixed parameter $a = 0.895$ by varying the slope angle φ showing the period-1 unstable limit cycle, (b) Variation of the module of the Jacobian matrix eigenvalues of the Poincaré map, and (c) Variation of the loci of the characteristic multipliers with respect to the unit circle, as varying the slope angle φ for $a = 0.895$.

unit circle through -1, indicating a period-doubling bifurcation. We observe in Figure 7(a) that the green eigenvalue leaves the unit circle via the real axis via the point -1, to mark hence the appearance of the period-doubling bifurcation and hence the beginning of the period-doubling scenario.

In Figure 8(a), we added the unstable solutions to the diagram that is shown in Figure 2(e) with a dashed magenta line. We see that the stable solution ends with a Neimark-Sacker bifurcation, but the diagram continues to evolve with unstable solutions until $\varphi = 12.44^\circ$. This Neimark-Sacker bifurcation is presented by the two eigenvalues green and cyan which take values greater than 1 in Figure 8(b), which presents the module of the eigenvalues of the Jacobian matrix of the Poincaré map. To show the Neimark-Sacker bifurcation well, we have presented the loci characteristic multipliers in Figure 8(c) where we see the location and variation of all the eigenvalues with respect to the unit circle.

Analysis through attractors

From a certain initial condition and for a set of parameters φ and a, the trajectory of the compass bipedal robot finally settles into an attractor state (in the state space). It can be a straightforward equilibrium point, a periodic trajectory (represented by a limit cycle in the phase plane or a some distinct points in the Poincaré section), a quasi-periodic trajectory (represented by a torus in the phase plane or a closed curve (like a closed circle) in the Poincaré section), or a strange/chaotic attractor, which is a type of trajectory on which a system moves from one situation to another without ever settling.

Attractors in the phase plane

Examples of periodic attractors in the phase plane and for different values of the two parameters a and φ, are shown in Figure 9(a), Figure 9(b), Figure 9(c), Figure 9(d) and Figure 9(e). They present respectively a 1-periodic attractor represented by a single closed trajectory, a 2-periodic attractor, a 4-periodic attractor, a 6-periodic attractor and an 8-periodic attractor.

We stated that the first attractor in Figure 9(a) plotted for $\varphi = 4^\circ$ clearly demonstrates that the step period of the biped robot's locomotion for $a = 0.5$ is 1-periodic as shown by a red arrow in Figure 2(a). The same remark for the second 2-periodic attractor of Figure 9(b), which supports the findings in Figure 2(b) for all the values of the parameter φ between 8.944° and 10.19° for $a = 0.895$ inside the bubble. The 4-periodic shape of Figure 9(c) is the attractor of the 4-periodic behavior of the compass-type bipedal robot shown in Figure 2(d) for $a = 0.8846$ and for the values of φ between 10.5° and 10.92°. The 6-periodic attractor in Figure 9(d) exhibited for $a = 0.87$ and $\varphi = 10.48^\circ$ reveals the 6-periodic behavior of the compass robot presented in Figure 2(b). For $a = 0.881$, which is comparable to what is depicted in Figure 2(c), we depict in Figure 9(e) an 8-periodic attractor.

Examples of chaotic attractors are shown in Figure 10(a), Figure 10(b), Figure 10(c) and Figure 10(d). All these diagrams present chaotic attractors, which are characterized by an infinity of unstable limit cycles embedded within it. These figures support what was reported about the bifurcation diagrams in the previous subsection.

Attractors in the Poincaré section

A useful methodology for investigating dynamic systems, such as the bipedal compass robot, is the Poincaré section. We concentrate on certain location along the system's trajectory that correlates to the point where the trajectory meets the hyperplan, which is the Poincaré section, rather than the continuous trajectory where the attractor is traced in the plane phase. For instance, if we have a 1-periodic behavior, we find a single point at which the 1-period trajectory intersects the Poincaré section. If we have a 2-periodic behavior, we find 2 points at which the system's trajectory intersects with the Poincaré section

We notice new shapes for the attractors in the Poincaré section in Figure 11. Due to the infinite number of points, a chaotic attractor is shown in the first plot in Figure 11(a). Additionally, Figure 11(b) displays an infinite number of points, but they all diverge outward, which is what attracts the behavior that is almost periodic due to the Neimark-Sacker bifurcation (NSB).

Analysis via Lyapunov exponents

The calculation of Lyapunov exponents is a numerical method that proves the existence of bifurcation in nonlinear dynamical systems. Moreover, they reveal the sensitive dependence of the dynamic system on neighboring initial conditions. Furthermore, the sign of the largest Lyapunov exponents demonstrates the type of the generated attractor, which can be either periodic or quasi-periodic or chaotic.

The computation of the spectrum of Lyapunov exponents for continuous-time as well as discrete-time dynamical systems has been widely investigated in several research works. A nonlinear dynamic system of dimension n has n Lyapunov exponents and for a smooth nonlinear dynamical system, the computation of the Lyapunov exponents becomes classic nowadays. For the hybrid impulsive nonlinear dynamics of the passive compass bipedal robot, and since the dimension of the state vector x is 4, then we have 4 Lyapunov exponents. Nevertheless, because of the impulsive and hybrid feature of the bipedal dynamics (17) of the passive compass robot, the computation of the Lyapunov exponents is complicated (Gritli and Belghith 2015, 2016a; Gritli *et al.* 2012). The calculation of the spectrum of Lyapunov exponents depends chiefly on the jump matrix $\mathcal{S}(x^+, x^-)$ that was defined by expression (49), and then on the fundamental solution matrix $\Phi^+(t, x_0)$. The computation of the spectrum of Lyapunov exponents for the passive compass bipedal robot and also for the semi-passive torso-driven bipedal robot has been achieved previously in (Gritli *et al.* 2012) and also using the explicit analytical expression of the controlled hybrid Poincaré map (Gritli and Belghith 2015, 2016a).

The variation of the four Lyapunov exponents λ_1, λ_2, λ_3, and λ_4 is shown in Figure 12(a) by adopting the lower-leg segment length $a = 0.5$ and then by varying the slope parameter φ from the value 4°. Evolution of the two largest Lyapunov exponents λ_1 and λ_2 with respect to φ is depicted in Figure 12(b). The largest Lyapunov exponent λ_1 is presented in blue whereas λ_2 is colored in red. When λ_1 takes the value 0 and while the other exponents are negative for the slope angle φ varies between 4° and 5.03°, this situation indicates hence that the passive bipedal walking of the compass robot is periodic. As it was presented in Figure 2(a), and for this same interval of the values of φ, we have a period doubling schema towards chaos. In Figure 12, this period-doubling scenario is presented by a succession of parabolic shapes formed by the two Lyapunov exponents λ_2 and λ_3. Each intersection of the second exponent λ_2 with the first one λ_1 i.e. with the value of 0, indicates the presence of a period-doubling bifurcation.

For the values of $\varphi > 5.03^\circ$ and referring to Figure 2(a), chaos starts to happen. In Figure 12, this complex behavior is presented by a positive value of the largest Lyapunov exponent λ_1. As φ increases, λ_1 increases as well. Furthermore, when the walking behavior is chaotic, the second Lyapunov exponent λ_2 takes the

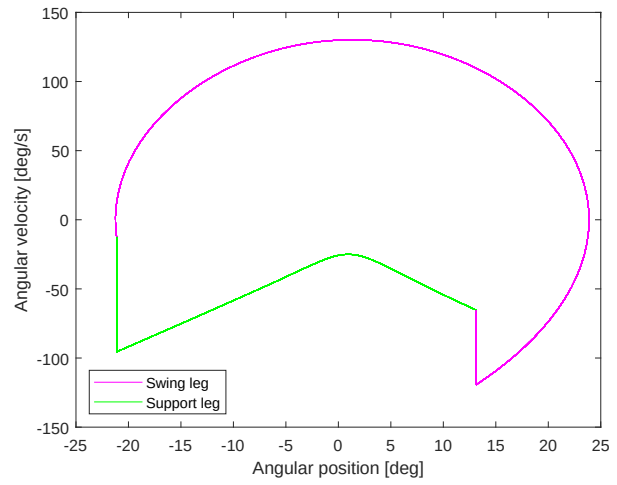

(a) 1-periodic attractor

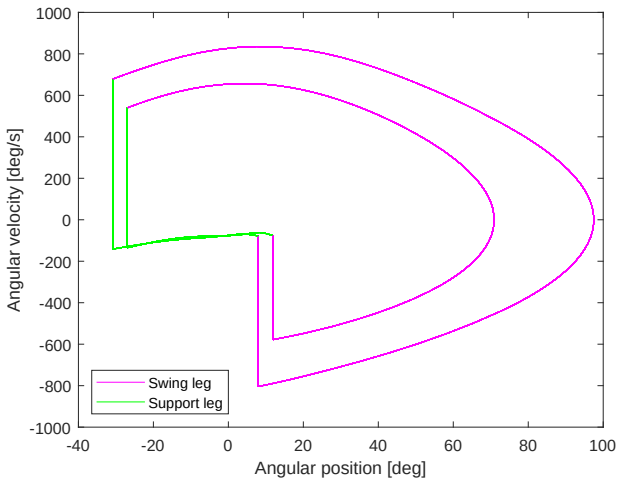

(b) 2-periodic attractor

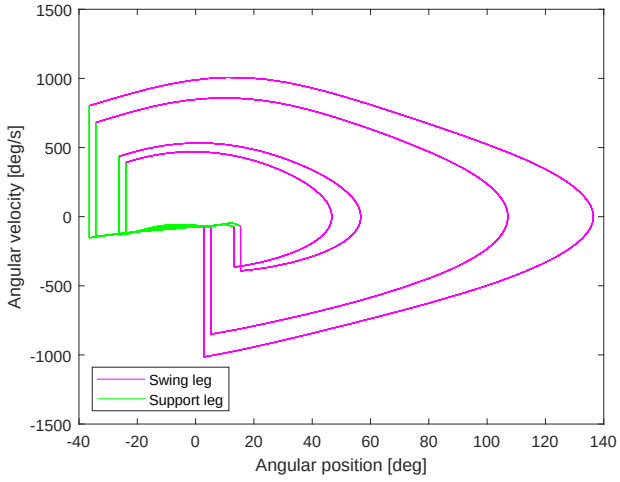

(c) 4-periodic attractor

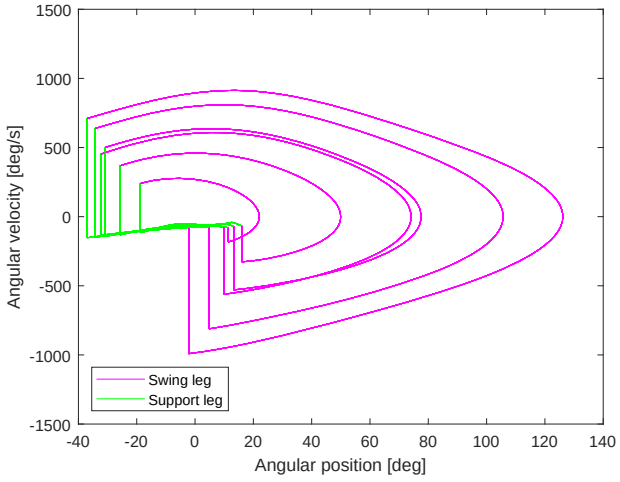

(d) 6-periodic attractor

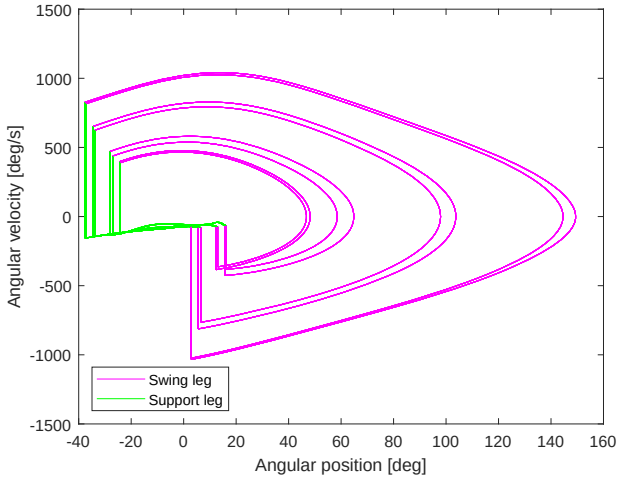

(e) 8-periodic attractor

Figure 9 Attractors in the phase plane: (a) A 1-periodic attractor for $a = 0.5$ and $\varphi = 4^\circ$, (b) A 2-periodic attractor for $a = 0.895$ and $\varphi = 9.5^\circ$, (c) A 4-periodic attractor for $a = 0.8846$ and $\varphi = 10.5^\circ$, (d) A 6-periodic attractor for $a = 0.87$ and $\varphi = 10.48^\circ$, and (e) An 8-periodic attractor for $a = 0.881$ and $\varphi = 10.75^\circ$.

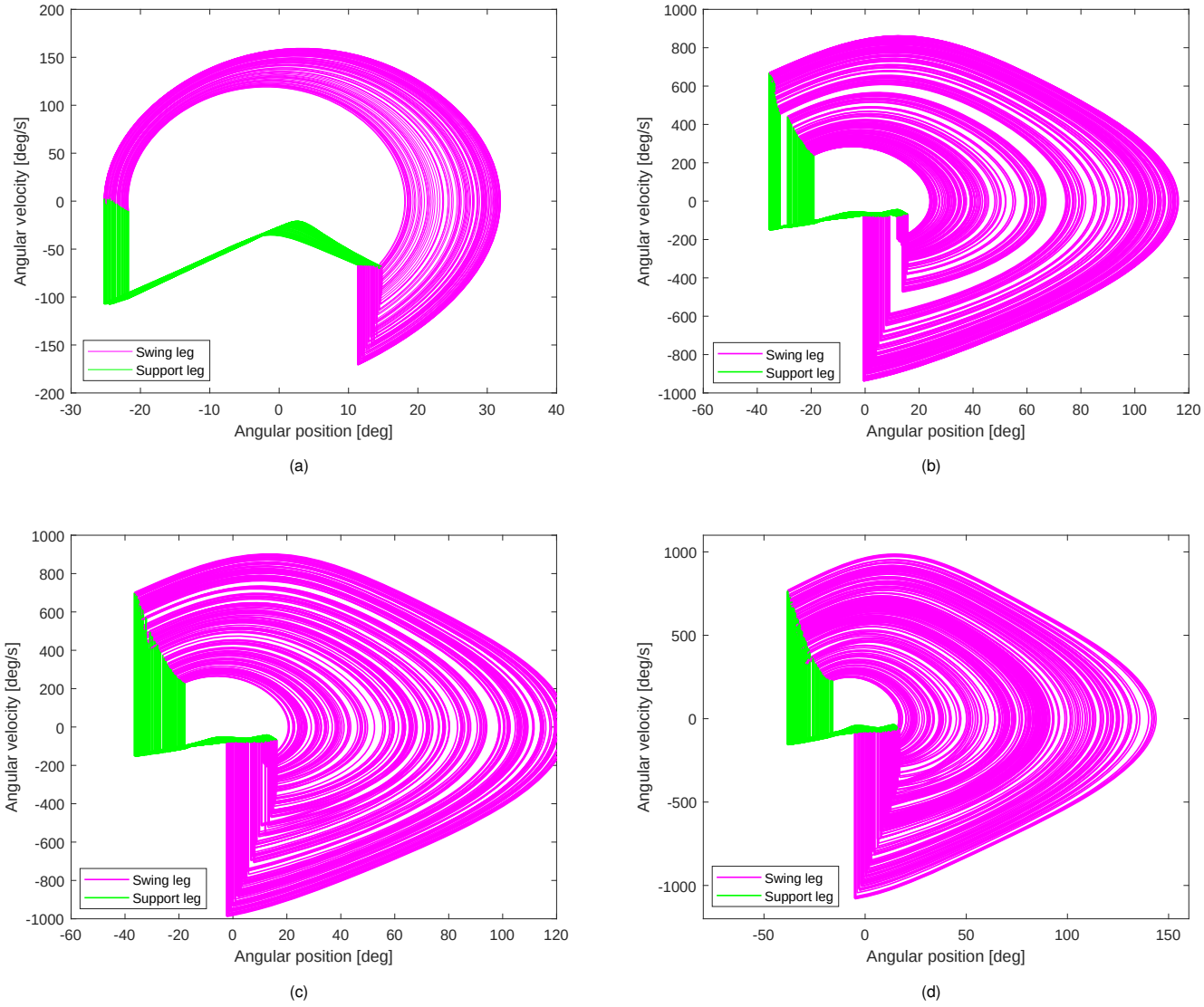

Figure 10 Chaotic attractors in the phase plane for (a) $a = 0.5$ and $\varphi = 5.2°$, (b) $a = 0.87$ and $\varphi = 9.85°$, (c) $a = 0.87$ and $\varphi = 10.1°$, and (d) $a = 0.87$ and $\varphi = 10.6°$. The portrait in (a) reveals the classical chaotic attractor that was observed for the classical parameter $a = 0.5$. The other plots show that the chaotic attractor becomes larger by varying/increasing the slope angle φ.

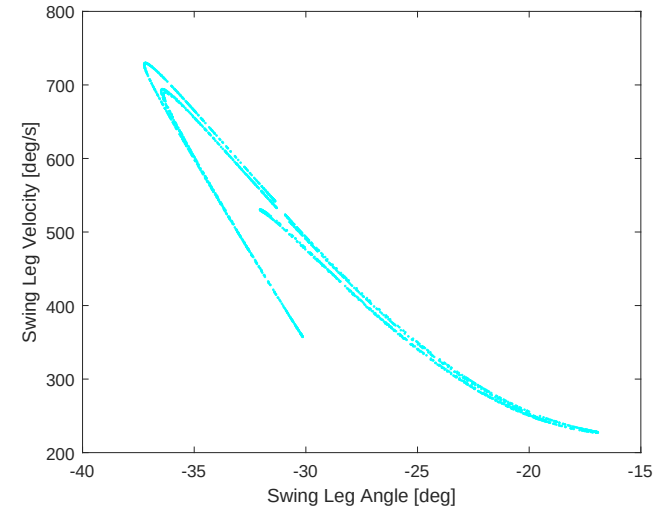

(a) A chaotic attractor

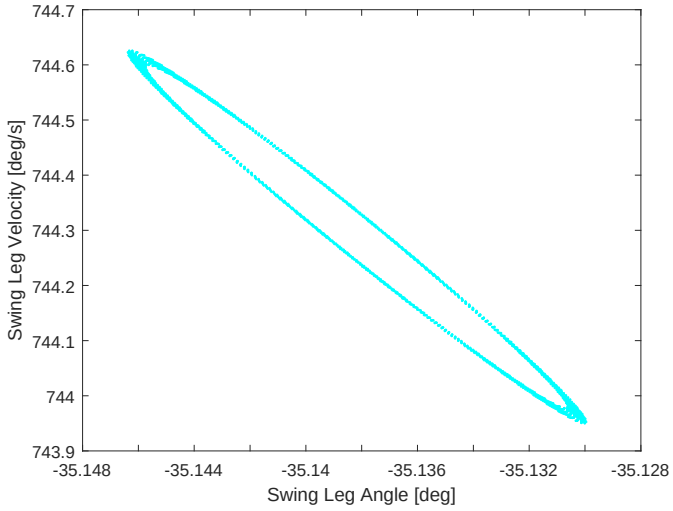

(b) A quasi-periodic attractor

Figure 11 Attractors in the Poincaré section for (a) chaotic attractor for $a = 0.87$ and $\varphi = 10.3°$, and (b) NSB attractor for$a = 0.8846$ and $\varphi = 12.21°$.

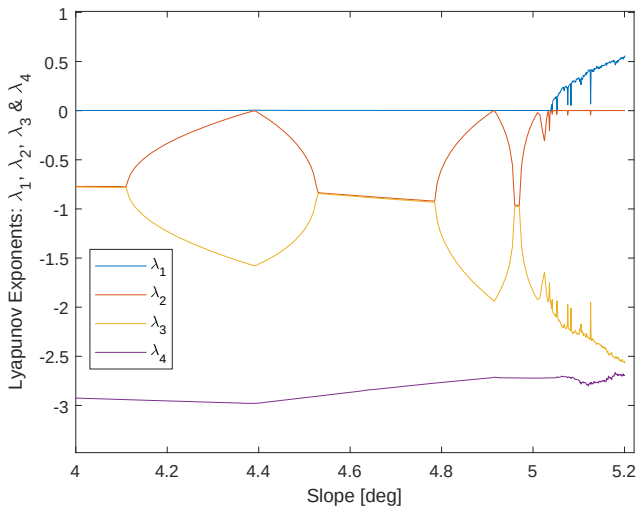

(a) $\lambda_1, \lambda_2, \lambda_3$ & λ_4

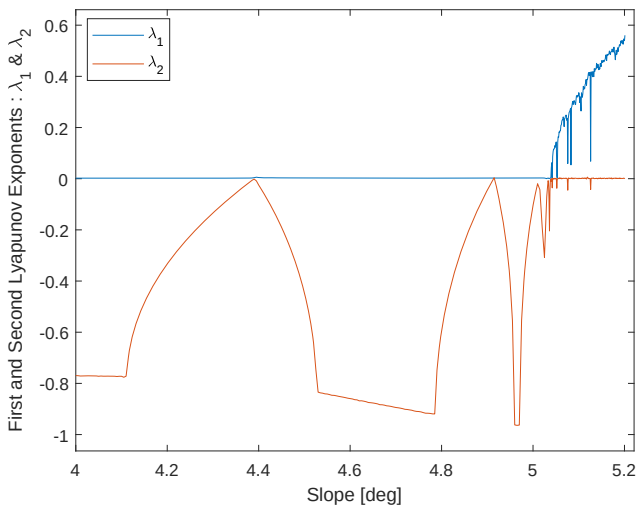

(b) λ_1 & λ_2

Figure 12 Variation of the Lyapunov exponents for $a = 0.5$ and by varying the slope angle of the walking surface φ from the value $4°$. (a) reveals the four Lyapunov exponents λ_1, λ_2, λ_3, and λ_4, whereas (b) shows the two largest Lyapunov exponents λ_1 and λ_2.

value 0, while the two other Lyapunov exponents λ_3 and λ_4 remain always negative.

It is important to note that within the chaotic regime, that is for $\varphi > 5.03°$, there are some fluctuations of the largest Lyapunov exponent λ_1 to zero. This behavior indicates the existence of periodicity windows inside the chaotic regime.

CONCLUSIONS

In this research study, we analyzed the passive gait of a planar biped robot using a motion that resembled a compass. We employed the bifurcation diagrams, the Poincaré sections, the phase planes and the variation of the characteristic multipliers to investigate the exhibited behaviors. Two different bifurcation parameters were considered: the parameter a which is the length of the lower leg segment and the parameter φ which is the slope angle of the inclined walking surface. We presented different simulation results to analyze the complex behavior of the passive dynamic bipedal walking of the compass robot. We demonstrated how the value of the parameter a can alter the stability and the overall behavior of the bipedal robot. We showed how the traditional period-doubling route to chaos can be transformed into a completely different behavior under some slight variation of the two parameters φ and a. In addition, we showed that the passive gait of the compass robot reveals the exhibition of the Neimark-Sacker bifurcation and hence the existence of the quasi-periodic passive gaits.

In our future research, the objective is to analyze the compass-gait walker's passive motion using the explicit analytical representation of the Poincaré map (Znegui *et al.* 2020a, 2021). In addition, our goal is to achieve an in-depth study of the Lyapunov exponents for different bifurcation diagrams and then for different scenarios that were presented in this paper.

Acknowledgments

The authors would like to thank the Ministry of Higher Education and Scientific Research (Ministère de l'Enseignement Supérieur et de la Recherche Scientifique (MESRS)), Tunisia, for technical and financial support under the PEJC Project no. 20PEJC 06-02.

Availability of data and material

Not applicable.

Conflicts of interest

The authors declare that there is no conflict of interest regarding the publication of this paper.

LITERATURE CITED

Added, E. and H. Gritli, 2020a Control of the passive dynamic gait of the bipedal compass-type robot through trajectory tracking. In *2020 20th International Conference on Sciences and Techniques of Automatic Control and Computer Engineering (STA)*, pp. 155–162.

Added, E. and H. Gritli, 2020b Trajectory design and tracking-based control of the passive compass biped. In *2020 4th International Conference on Advanced Systems and Emergent Technologies (IC_ASET)*, pp. 417–424.

Added, E. and H. Gritli, 2022 Birth of the Neimark–Sacker bifurcation for the passive compass-gait walker. In *Advances in Nonlinear Dynamics*, edited by W. Lacarbonara, B. Balachandran, M. J. Leamy, J. Ma, J. A. Tenreiro Machado, and G. Stepan, pp. 683–697, Cham, Springer International Publishing.

Added, E. and H. Gritli, 2023 A further analysis of the passive compass-gait bipedal robot and its period-doubling route to chaos. In *New Perspectives on Nonlinear Dynamics and Complexity*, edited by D. Volchenkov and A. C. J. Luo, pp. 11–30, Cham, Springer International Publishing.

Added, E., H. Gritli, and S. Belghith, 2021a Additional complex behaviors, bifurcations and chaos, in the passive walk of the compass-type bipedal robot. IFAC-PapersOnLine **54**: 111–116, 6th IFAC Conference on Analysis and Control of Chaotic Systems CHAOS 2021.

Added, E., H. Gritli, and S. Belghith, 2021b Further analysis of the passive dynamics of the compass biped walker and control of chaos via two trajectory tracking approaches. Complexity **2021**: 5533451 (39 pages).

Added, E., H. Gritli, and S. Belghith, 2021c Further analysis of the passive walking gaits of the compass biped robot: Bifurcations and chaos. In *2021 18th International Multi-Conference on Systems, Signals & Devices (SSD)*, pp. 160–165.

Added, E., H. Gritli, and S. Belghith, 2022a Trajectory tracking-based control of the chaotic behavior in the passive bipedal compass-type robot. The European Physical Journal Special Topics **231**: 1071–1084.

Added, E., H. Gritli, and S. Belghith, 2022b Trajectory tracking control of the compass-type bipedal robot gait via an improved PD+ controller. In *2022 5th International Conference on Advanced Systems and Emergent Technologies (IC_ASET)*, pp. 482–488.

Akgul, A., S. Hussain, and I. Pehlivan, 2016 A new three-dimensional chaotic system, its dynamical analysis and electronic circuit applications. Optik - International Journal for Light and Electron Optics **127**: 7062 – 7071.

Andrievskii, B. R. and A. L. Fradkov, 2003 Control of chaos: Methods and applications. I. Methods. Automation and Remote Control **64**: 673–713.

Andrievskii, B. R. and A. L. Fradkov, 2004 Control of chaos: Methods and applications. II. Applications. Automation and Remote Control **65**: 505–533.

Aricioğlu, M. A. and O. N. Berk, 2022 A comparative proposal on learning the chaos to understand the environment. Chaos Theory and Applications **4**: 19 – 25.

Azar, A. T., C. Volos, N. A. Gerodimos, G. S. Tombras, V.-T. Pham, *et al.*, 2017 A novel chaotic system without equilibrium: Dynamics, synchronization, and circuit realization. Complexity **2017**: 7871467.

Bekey, G. A. and K. Y. Goldberg, 2012 *Neural networks in robotics*, volume 202. Springer Science & Business Media.

Beritelli, F., E. Di Cola, L. Fortuna, and F. Italia, 2000 Multilayer chaotic encryption for secure communications in packet switching networks. In *WCC 2000-ICCT 2000. 2000 International Conference on Communication Technology Proceedings (Cat. No. 00EX420)*, volume 2, pp. 1575–1582.

Boccaletti, S., C. Grebogi, Y.-C. Lai, H. Mancini, and D. Maza, 2000 The control of chaos: theory and applications. Physics Reports **329**: 103–197.

Boubaker, O. and S. Jafari, 2019 *Recent Advances in Chaotic Systems and Synchronization: From Theory to Real World Applications*. Emerging Methodologies and Applications in Modelling, Identification and Control, Elsevier, first edition.

Buscarino, A., C. Famoso, L. Fortuna, and M. Frasca, 2016 A new chaotic electro-mechanical oscillator. International Journal of Bifurcation and Chaos **26**: 1650161.

Chevallereau, C., G. Bessonnet, G. Abba, and Y. Aoustin, 2009 *Bipedal Robots: Modeling, Design and Walking Synthesis*. John Wiley & Sons, Wiley-ISTE, first edition.

Collins, S., A. Ruina, R. Tedrake, and M. Wisse, 2005 Efficient bipedal robots based on passive-dynamic walkers. Science **307**: 1082–1085.

Deng, K., M. Zhao, and W. Xu, 2017 Passive dynamic walking with a torso coupled via torsional springs. International Journal of Humanoid Robotics **13**: 1650024.

Fathizadeh, M., H. Mohammadi, and S. Taghvaei, 2019 A modified passive walking biped model with two feasible switching patterns of motion to resemble multi-pattern human walking. Chaos, Solitons & Fractals **127**: 83 – 95.

Fathizadeh, M., S. Taghvaei, and H. Mohammadi, 2018 Analyzing bifurcation, stability and chaos for a passive walking biped model with a sole foot. International Journal of Bifurcation and Chaos **28**: 1850113.

Ferreira, B. B., A. S. de Paula, and M. A. Savi, 2011 Chaos control applied to heart rhythm dynamics. Chaos, Solitons & Fractals **44**: 587–599.

Firth, W., 1991 Chaos–predicting the unpredictable. BMJ: British Medical Journal **303**: 1565.

Fradkov, A. L. and R. J. Evans, 2005 Control of chaos: Methods and applications in engineering. Annual Reviews in Control **29**: 33–56.

Fradkov, A. L., R. J. Evans, and B. R. Andrievsky, 2006 Control of chaos: Methods and applications in mechanics. Philosophical Transactions of The Royal Society A **364**: 2279–2307.

Garcia, M., A. Chatterjee, and A. Ruina, 2000 Efficiency, speed, and scaling of two-dimensional passive-dynamic walking. Dynamics and Stability of Sytems **15**: 75–99.

Garcia, M., A. Chatterjee, A. Ruina, and M. Coleman, 1998 The simplest walking model: Stability, complexity, and scaling. Journal of Biomechanical Engineering **120**: 281–288.

Goswami, A., B. Thuilot, and B. Espiau, 1996 *Compass-like biped*

robot. Part I: Stability and bifurcation of passive gaits, volume 2996. Technical Report, INRIA.

Goswami, A., B. Thuilot, and B. Espiau, 1998 Study of the passive gait of a compass-like biped robot: Symmetry and chaos. International Journal of Robotics Research **17**: 1282–1301.

Goswami, A. and P. Vadakkepat, 2019 *Humanoid Robotics: A Reference*. Springer Netherlands, first edition.

Grassi, G., 2021 Chaos in the real world: Recent applications to communications, computing, distributed sensing, robotic motion, bio-impedance modelling and encryption systems. Symmetry **2021**: 2151.

Grebogi, C., Y.-C. Lai, and S. Hayes, 1997 Control and applications of chaos. Journal of the Franklin Institute **334**: 1115–1146, Visions of Nonlinear Mechanics in the 21st Century.

Gritli, H. and S. Belghith, 2015 Computation of the Lyapunov exponents in the compass-gait model under OGY control via a hybrid Poincaré map. Chaos, Solitons & Fractals **81**: 172–183.

Gritli, H. and S. Belghith, 2016a Bifurcations and chaos in the semi-passive bipedal dynamic walking model under a modified OGY-based control approach. Nonlinear Dynamics **83**: 1955–1973.

Gritli, H. and S. Belghith, 2016b Displayed phenomena in the semi-passive torso-driven biped model under OGY-based control method: Birth of a torus bifurcation. Applied Mathematical Modelling **40**: 2946–2967.

Gritli, H. and S. Belghith, 2017a Walking dynamics of the passive compass-gait model under OGY-based control: Emergence of bifurcations and chaos. Communications in Nonlinear Science and Numerical Simulation **47**: 308–327.

Gritli, H. and S. Belghith, 2017b Walking dynamics of the passive compass-gait model under OGY-based state-feedback control: Analysis of local bifurcations via the hybrid Poincaré map. Chaos, Solitons & Fractals **98**: 72 – 87.

Gritli, H. and S. Belghith, 2018a Diversity in the nonlinear dynamic behavior of a one-degree-of-freedom impact mechanical oscillator under OGY-based state-feedback control law: order, chaos and exhibition of the border-collision bifurcation. Mechanism and Machine Theory **124**: 1–41.

Gritli, H. and S. Belghith, 2018b Walking dynamics of the passive compass-gait model under OGY-based state-feedback control: Rise of the Neimark–Sacker bifurcation. Chaos, Solitons & Fractals **110**: 158 – 168.

Gritli, H., S. Belghith, and N. Khraeif, 2012 Intermittency and interior crisis as route to chaos in dynamic walking of two biped robots. International Journal of Bifurcation and Chaos **22**: 1250056.

Gritli, H., S. Belghith, and N. Khraeif, 2015 OGY-based control of chaos in semi-passive dynamic walking of a torso-driven biped robot. Nonlinear Dynamics **79**: 1363–1384.

Gritli, H., N. Khraeif, and S. Belghith, 2011 Cyclic-fold bifurcation in passive bipedal walking of a compass-gait biped robot with leg length discrepancy. In *2011 IEEE International Conference on Mechatronics*, pp. 851–856.

Gritli, H., N. Khraeif, and S. Belghith, 2013 Chaos control in passive walking dynamics of a compass-gait model. Communications in Nonlinear Science and Numerical Simulation **18**: 2048–2065.

Gritli, H., N. Khraief, and S. Belghith, 2018 Complex walking behaviours, chaos and bifurcations of a simple passive compass-gait biped model suffering from leg length asymmetry. International Journal of Simulation and Process Modelling **13**: 446–462.

Grizzle, J. W., G. Abba, and F. Plestan, 2001 Asymptotically stable walking for biped robots: Analysis via systems with impulse effects. IEEE Transaction on Automatic Control **46**: 51–64.

Guanrong, C., 2021 Chaos theory and applications: a new trend. Chaos Theory and Applications **3**: 1–2.

Gupta, S. and A. Kumar, 2017 A brief review of dynamics and control of underactuated biped robots. Advanced Robotics **31**: 607–623.

Harrison, R. C., A. OLDAG, E. PERKİNS, *et al.*, 2022 Experimental validation of a chaotic jerk circuit based true random number generator. Chaos Theory and Applications **4**: 64–70.

Iqbal, S., X. Z. Zang, Y. H. Zhu, and J. Zhao, 2014 Bifurcations and chaos in passive dynamic walking: A review. Robotics and Autonomous Systems **62**: 889–909.

Jimenez, A., E. N. Sanchez, G. Chen, and J. P. Perez, 2009 Real-time chaotic circuit stabilization via inverse optimal control. International Journal of Circuit Theory and Applications **37**: 887–898.

Jun, M., 2022 Chaos theory and applications: the physical evidence, mechanism are important in chaotic systems. Chaos Theory and Applications **4**: 1–3.

Khraief Haddad, N., S. Belghith, H. Gritli, and A. Chemori, 2017 From hopf bifurcation to limit cycles control in underactuated mechanical systems. International Journal of Bifurcation and Chaos **27**: 1750104.

Kuo, A. D., 2007 The six determinants of gait and the inverted pendulum analogy: A dynamic walking perspective. Human Movement Science **26**: 617 – 656.

Li, T.-Y. and J. A. Yorke, 2004 Period three implies chaos. In *The theory of chaotic attractors*, pp. 77–84, Springer.

Makarenkov, O., 2020 Existence and stability of limit cycles in the model of a planar passive biped walking down a slope. Proceedings of the Royal Society A: Mathematical, Physical and Engineering Sciences **476**: 20190450.

McGeer, T., 1990 Passive dynamic walking. International Journal of Robotics Research **9**: 62–82.

Meng, M. Q.-H. and R. Song, 2022 Legged mobile robots for challenging terrains. Biomimetic Intelligence and Robotics **2**: 100034.

Miladi, Y., A. Chemori, and M. Feki, 16-19 March 2015 The compass-like biped robot revisited: Nonlinear control of the disturbed passive dynamic walking. In *2015 IEEE 12th International Multi-Conference on Systems, Signals Devices (SSD15)*, pp. 1–7, Mahdia, Tunisia.

Miladi, Y., N. Derbel, and M. Feki, 2021 Optimal control based on multiple models approach of chaotic switched systems, application to a stepper motor. International Journal of Automation and Control **15**: 240–258.

Montazeri Moghadam, S., M. Sadeghi Talarposhti, A. Niaty, F. Towhidkhah, and S. Jafari, 2018 The simple chaotic model of passive dynamic walking. Nonlinear Dynamics **93**: 1183–1199.

Nourian Zavareh, M., F. Nazarimehr, K. Rajagopal, and S. Jafari, 2018 Hidden attractor in a passive motion model of compass-gait robot. International Journal of Bifurcation and Chaos **28**: 1850171.

Ott, E., C. Grebogi, and J. A. Yorke, 1990 Controlling chaos. Physical review letters **64**: 1196–1199.

Reher, J. and A. D. Ames, 2021 Dynamic walking: Toward agile and efficient bipedal robots. Annual Review of Control, Robotics, and Autonomous Systems **4**: 535–572.

Sambas, A., S. Vaidyanathan, M. Mamat, W. Sanjaya, and D. S. Rahayu, 2016 A 3-d novel jerk chaotic system and its application in secure communication system and mobile robot navigation. In *Advances and applications in Chaotic systems*, pp. 283–310, Springer.

Sprott, J., 2020 Do we need more chaos examples? Chaos Theory

and Applications **2**: 49 – 51.
Vaidyanathan, S., M. Feki, A. Sambas, and C.-H. Lien, 2018 A new biological snap oscillator: its modelling, analysis, simulations and circuit design. International Journal of Simulation and Process Modelling **13**: 419–432.
Vaidyanathan, S., A. Sambas, M. Mamat, and W. M. Sanjaya, 2017 A new three-dimensional chaotic system with a hidden attractor, circuit design and application in wireless mobile robot. Archives of Control Sciences **27**: 541–554.
Volos, C., A. Akgul, V.-T. Pham, I. Stouboulos, and I. Kyprianidis, 2017 A simple chaotic circuit with a hyperbolic sine function and its use in a sound encryption scheme. Nonlinear Dynamics **89**: 1047–1061.
Volos, C. K., I. M. Kyprianidis, and I. N. Stouboulos, 2012 A chaotic path planning generator for autonomous mobile robots. Robotics and Autonomous Systems **60**: 651–656.
Volos, C. K., I. M. Kyprianidis, and I. N. Stouboulos, 2013 Experimental investigation on coverage performance of a chaotic autonomous mobile robot. Robotics and Autonomous Systems **61**: 1314–1322.
Walter, S., 2014 Poincaré on clocks in motion. Studies in History and Philosophy of Science Part B: Studies in History and Philosophy of Modern Physics **47**: 131–141.
Westervelt, E. R., J. W. Grizzle, C. Chevallereau, J.-H. Choi, and B. Morris, 2007 *Feedback control of dynamic bipedal robot locomotion*. Taylor & Francis/CRC, London.
Xiaoting, Y., Y. Liguo, and W. Zhouchao, 2022 Stability and hopf bifurcation analysis of a fractional-order leslie-gower prey-predator-parasite system with delay. Chaos Theory and Applications **4**: 71–81.
Xie, Y., B. Lou, A. Xie, and D. Zhang, 2020 A review: Robust locomotion for biped humanoid robots. Journal of Physics: Conference Series **1487**: 012048.
Yang, D. and J. Zhou, 2014 Connections among several chaos feedback control approaches and chaotic vibration control of mechanical systems. Communications in Nonlinear Science and Numerical Simulation **19**: 3954–3968.
Znegui, W., H. Gritli, and S. Belghith, 2020a Design of an explicit expression of the Poincaré map for the passive dynamic walking of the compass-gait biped model. Chaos, Solitons & Fractals **130**: 109436.
Znegui, W., H. Gritli, and S. Belghith, 2020b Stabilization of the passive walking dynamics of the compass-gait biped robot by developing the analytical expression of the controlled Poincaré map. Nonlinear Dynamics **101**: 1061–1091.
Znegui, W., H. Gritli, and S. Belghith, 2021 A new Poincaré map for analysis of complex walking behavior of the compass-gait biped robot. Applied Mathematical Modelling **94**: 534–557.
Öztürk, H., 2020 A novel chaos application to observe performance of asynchronous machine under chaotic load. Chaos Theory and Applications **2**: 90 – 97.

How to cite this article: Added, E., Gritli, H., and Belghith, S. Occurrence of Complex Behaviors in the Uncontrolled Passive Compass Biped Model. *Chaos Theory and Applications*, 4(4), 246-266, 2022.